scientific reports

Check for updates

OPEN

Investigating the effects of microwave plasma on bacterial cell structures, viability, and membrane integrity

Tejal Barkhade[1,4]✉, Kushagra Nigam[1], Ganesh Ravi[1,2], Seema Rawat[3] & Sudhir Kumar Nema[1,2]

Plasma-mediated bacterial inactivation holds great promise but presents several challenges. This study investigates the antibacterial effect of 2.45 GHz non-thermal microwave (MW) plasma on *Staphylococcus aureus* (*S. aureus*) and *Salmonella abony* (*S. abony*) suspended in phosphate-buffered saline (PBS). A 6-log reduction in both bacterial strains was achieved within 300 s of plasma exposure. The enhanced inactivation is attributed to elevated levels of reactive oxygen species (ROS), particularly $^{\cdot}OH$ (30.30% in *S. aureus*, 40.13% in *S. abony*) and H_2O_2 (173.27% in *S. aureus*, and 391.84% in *S. abony*), which caused oxidative stress and membrane depolarization, detected via fluorescence spectrofluorometry. Morphological changes were confirmed through field emission scanning electron microscopy (FE-SEM). Membrane impairment led to leakage of intracellular contents such as proteins, lipids, and nucleic acids. DNA damage was evident from hyperchromic effects observed at 260 nm. Confocal microscopy revealed a qualitative increase in red fluorescent (dead) cells with longer exposure. Flow cytometry further quantified the dead cells at 88% in *S. aureus* and 95% in *S. abony*. These findings provide comprehensive insight into the bacterial inactivation mechanism and demonstrate the strong potential of non-thermal MW plasma for applications in sterilization, infection control, and food safety.

Keywords Inactivation, Microwave plasma, Bacteria, *S. aureus*, *S. abony*, Reactive oxygen species

Non-thermal plasma holds immense promise in revolutionizing antimicrobial treatment across various healthcare domains. Its potential applications are expansive, offering a versatile approach to controlling microbial infection in diverse settings and scenarios through sterilization processes[1–7]. While conventional sterilizing methods like heat, chemical disinfectants, and radiation have long been the mainstay of infection control in healthcare facilities, they do come with inherent limitations such as incompatibility with heat-sensitive materials, toxicity, and radiation[6]. Given these limitations, researchers and scientists have explored alternative sterilization techniques, including plasma-based treatments, which offer a more effective, non-toxic, and environmentally sustainable approach compatible with various materials and applications[8]. Plasma's unique composition, consisting of ions, electrons, and neutral particles, enables the generation of reactive species capable of neutralizing a wide array of microorganisms[9–11]. The generation of reactive oxygen and nitrogen species ($^{\cdot}OH$, H_2O_2, O, O_3, and NO) exert a lethal effect on the bacterial cell, creating oxidative stress, disrupting membrane and inflicting DNA damage[12–14]. Factors such as the duration of plasma exposure, energy source, pressure, gas type and flow rate and distance from the plasma source play a critical role in determining the effectiveness of the microbial treatment[15–17].

Consequently, investigations on plasma has undergone for microbial inactivation in diverse biomedical contexts. For example, Menashi et al. were the first to introduce pulsed plasma in 1968 and patented the technology for sterilizing glass surfaces, marking a significant milestone in this field[18]. Subsequently, various types of plasma have also been generated by scientists from different energy sources, such as alternating current (AC), direct current (DC), high frequency (HF), and radio frequency (RF), under varying atmospheric conditions and have

[1]Facilitation Centre for Industrial Plasma Technologies, Institute for Plasma Research, Gandhinagar, Gujarat 382428, India. [2]Homi Bhabha National Institute, Training School Complex, Anushaktinagar, Mumbai 400094, India. [3]School of Life Sciences, Central University of Gujarat, Gandhinagar, Gujarat 382030, India. [4]Department of Life Sciences, Parul Institute of Applied Sciences, Parul University, Vadodara, Gujarat 391760, India. ✉email: tejalbarkhade04@gmail.com; tejal.barkhade37399@paruluniversity.ac.in

been employed for antimicrobial treatments[19–21]. However, there is still a lack of an understanding of effects of these plasma sources at the molecular and genetic levels and considerable debate is going on regarding how different process parameters and the specific actions of various species involved in the process influence the overall outcome.

Among other plasma sources, microwave plasma stands out as a highly efficient and promising technology due to its near-instantaneous generation time, non-invasive nature, relatively simple power supply topology, and comparatively higher plasma densities (~ 10^{10} to 10^{11} per cc), which contribute to faster bacterial inactivation[22]. Compared to other forms of plasma, microwave plasma offers higher energy efficiency, uniform energy distribution, and rapid action, making it particularly suitable for time-sensitive applications[23]. Microwave plasma technology have been started growing slowly since few years, but it has not yet been commercialized due to the lack of understanding of the biochemical actions and mechanisms behind its microbial inactivation[8]. To gain a detailed understanding of plasma and microbial interactions, further research is needed. Though, some reported literature suggested the effectiveness of microwave plasma for antimicrobial treatment. For example, Renoux et al. used atmospheric microwave plasma (axial injection torch) argon for the inactivation of *E. coli* without thermal effect and demonstrated 4.2- Log reduction[24]. Handorf et al. observed that treating *Candida albicans* biofilms with a microwave-induced plasma torch resulted in a 77% reduction in viability after 20 s of treatment and a 90% reduction in metabolism after 40 s of treatment[25]. Moreau et al. applied an afterglow microwave discharge at 2.45 GHz and 180 W power under 1–9 mBar pressure to *Bacillus subtilis* endospores. Pure argon and a mixture of N_2/O_2 were used and a 6-log reductions was achieved in 40 min[26]. In another clinical study, Seo et al. collected various oral pathogens from saliva and inactivated them using microwave-pulsed non-thermal atmospheric pressure plasma, suggesting it as a useful alternative tool for the clinical treatment of periodontal diseases[27]. Kim et al. conducted an in vitro study on the antimicrobial activity of cold atmospheric microwave plasma against bacteria responsible for canine skin and ear infections. They achieved a 6-log reduction inactivation within 240 s at 50 W[28]. Most of the mentioned and other reported studies on microwave plasma have focused on bacterial viability reduction. However, neither study comprehensively and systematically analyzed non-thermal microwave plasma induced bacterial membrane depolarization, intracellular leakage, production of ROS, morphological analysis, dead assay, and DNA damage using multiple analytical techniques and it is not been extensively detailed in prior research. Thus, the purpose of our research is to deepen the understanding of bacterial inactivation at the molecular level, supporting our new findings.

In our previous work, we have investigated the antibacterial activity of direct current plasma and achieved 6-log reduction of Gram positive *S. aureus* and Gram negative *S. abony*. We also conducted detailed examinations of plasma-induced production of reactive species such as $^{\cdot}OH$ and H_2O_2, and their impact on bacterial inactivation. These analyses were carried out using various techniques including Spectrofluorometry, ATR-FTIR, Circular Dichroism spectroscopy, and FE-SEM[29]. The positive outcomes from our studies on effects of DC plasma on bacterial cells and limited literature demonstrating the efficiency of microwave plasma, influenced the development of microwave based plasma system. The novelty of present study lies in the use of a unique non-thermal microwave plasma installation operating at 2.45 GHz under a sub-atmospheric pressure of 0.3–0.5 mbar with an air-ozone mixture, enabling efficient bacterial inactivation. In addition, previous studies have utilized various gases to generate plasma and required longer exposure times for bacterial inactivation. In contrast, the present study demonstrates a 6-log reduction within just 300 s without the need for an external gas supply. Additionally, we provide a comparative analysis of bacterial inactivation at different plasma exposure times, offering new insights into the mechanistic actions of microwave plasma on both Gram-positive and Gram-negative bacteria. Our approach enhances bacterial inactivation which may have transformative impact on healthcare and beyond. Since microwave plasma density is directly proportional to the square of the frequency, it produces a greater concentration of reactive species[30].

The key points that push the frontier of knowledge are (i) indicating the advantages of sub-atmospheric microwave plasma (ii) providing new insights into bacterial membrane depolarization and intracellular leakage (iii) creating a correlation between CFU-based viability assays, flow cytometry and confocal images analysis, ensuring more reliable assessments of bacterial death (iv) quantifying ROS-mediated cell damage and DNA disruption (v) highlighting the improvements in microwave plasma sterilization processes for sustainable alternative to heat, radiation and chemical-based methods, reducing environmental impact while maintaining high efficiency. These methodologies proved effective in evaluating the significant mechanisms and non-thermal microwave plasma actions involved in the comparative inactivation of both Gram-positive and Gram-negative bacteria.

Material and methods

Chemicals, media and bacterial strains

Propidium iodide (PI, ≥ 94.0%), 3,3′-Diethyloxacarbocyanine iodide ($DiOC_2(3)$, 98%), 2′,7′- Dichlorofluorescin diacetate (DCFH-DA, ≥ 97%), Glutaraldehyde solution (25% in H_2O), Terephthalic acid (TA, 98%), Osmium tetroxide (≥ 99.8%), Dimethyl sulfoxide (DMSO), Phosphate Buffer Saline (PBS, pH-7.4), analytical reagent grade acetone and isopropyl alcohol were procured from Sigma Aldrich. For bacterial cultivation, standard nutrient agar (M001) and nutrient broth (M002) from HiMedia Laboratories were used. All culture media intended for microbiological analysis underwent autoclaving for 30 min at 15 psi and 121 °C. Bacterial strains, including *Staphylococcus aureus* (NCIM 2079) and *Salmonella abony* (NCIM 2257), were procured from the National Collection of Industrial Microorganisms (NCIM) at the National Chemical Laboratory in Pune, India. In this study, the term 'control' refers to an untreated bacterial suspension, maintained without exposure to plasma or ozone. This control helps as a reference to assess the effects of plasma treatment.

Non-thermal microwave plasma sterilization system

Figure 1 shows several components of microwave source based plasma sterilization system. These components include vacuum chamber, vacuum pump, bellow, ozone generator and pirani gauge with sensing gauge head for chamber pressure sensing, optical emission spectrometer (OES), laptop for OES data acquisition, optical fibre probe, needle valve for injection of working gas, vent valve for venting the system to atmospheric pressure after sterilization, tray for placing the bacterial suspension, 2.45 GHz microwave magnetron, microwave waveguide and antenna system, plunger disc for tuning the microwaves. A rotary pump (Model: INDVAC IVP 250) is utilized to lower the pressure in the sterilization chamber from atmospheric pressure (1 bar) to a sub-atmospheric level of approximately 0.015–0.02 mbar. Pressure readings are provided by a Pirani gauge (Model: DPHG-011), which operates on the Wheatstone bridge principle to measure resistance changes caused by the drop in chamber pressure. Once the desired base pressure is reached, a mixture of air and ozone is introduced into the chamber through a needle valve (Pfeiffer Make: EVN 116). This mixture, containing 0.8% ozone and 99.2% air, is produced by an ozonizer (Eltech Ozone Model: E1-O2-A-3GM), which draws in atmospheric air at a rate of 5 L per minute (LPM) and generates ozone (O_3) at a rate of 50 mg/min. Ozone plays a significant role in plasma sterilization by enhancing the antimicrobial effects through several mechanisms. When ozone reacts with other chemical species, such as H_2O_2, it generates reactive $^{\cdot}OH$[31,32]. These highly reactive molecules can further attack bacterial cells. Furthermore, the combination of ozone and plasma generates a synergistic effect for improving sterilization process[33].

The ozone and air mixture was injected as a precursor gas under low-pressure conditions (0.3–0.5 mbar). Once this pressure was stabilized, the microwave plasma was ignited. Operating at reduced pressure lowers the breakdown voltage required for plasma generation, facilitating stable plasma ignition and sustaining high-density discharge. Also, low pressure enhances the mean free path of electrons, leading to increased ionization efficacy and greater production of ROS, especially $^{\cdot}OH$ and H_2O_2, which are essential for bacterial inactivation.

Optical emission spectroscopy (OES)

Analysis is done on a variety of species produced in the air and ozone plasma created by a microwave source supply inside a sterilising system. A comprehensive optical spectrometer with a wavelength range of 300–1000 nm (ASEQ instruments, Canada made, model: UVH-1) with an adjustable slit (10–50 µm) and an optical resolution of less than 0.8 nm is used for the analysis. The fibre optic cable that was utilised for the in situ measurements was housed inside a quartz type A window-terminated stainless steel shaft[34].

Growing bacterial cultures

The strains of *S. aureus* (NCIM 2079) and *S. abony* (NCIM 2257) were utilized in the experiments. To revive freeze-dried bacterial cultures and for their cultivation, standard microbiological procedure was utilized. The freeze-dried cultures enclosed within glass ampoules were cautiously unsealed under sterile conditions, and

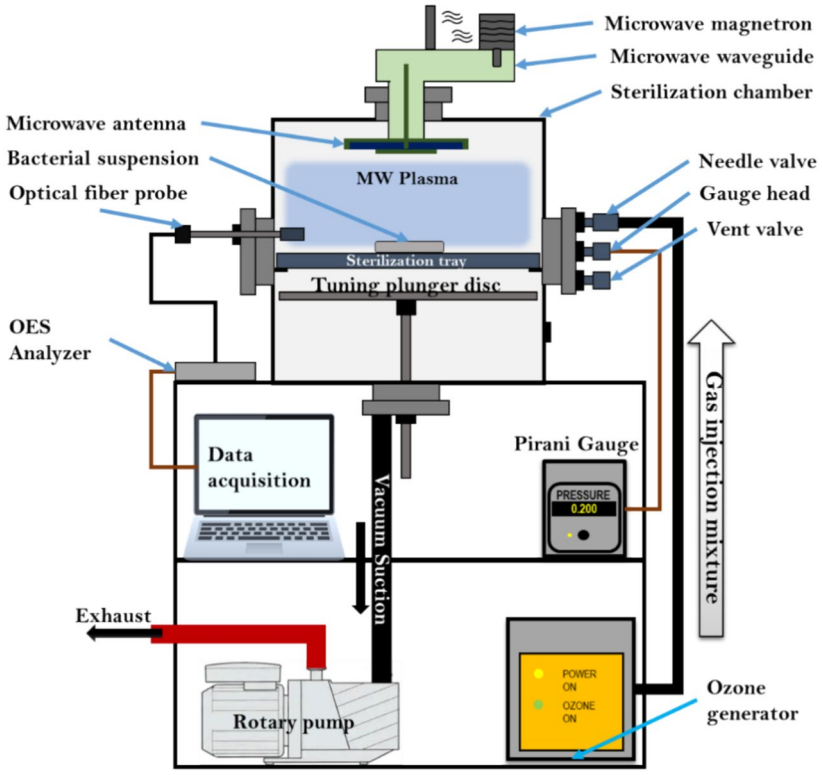

Fig. 1. Schematic of non-thermal microwave plasma system.

PBS was introduced to create a suspension of the cultures. Subsequently, the cultures were streaked on nutrient agar plates and incubated at 37 °C for 24 h. The pure culture was then preserved as glycerol stocks at -80 °C in a suitable medium supplemented with 50% glycerol[35].

Preparing bacterial cell suspension for plasma treatment

First, a single isolated colony of bacteria that had been previously revived was added in nutrient broth medium and incubated overnight at 37 °C and 250 rpm in a rotary shaker incubator. The bacterial density was adjusted to 10^6 colony-forming units per mL (CFU/mL) using multi-mode plate reader (Biotek Synergy H1 Hybrid Reader). The bacterial cells were then carefully harvested through centrifugation at 12,000 rpm for 5 min. The harvested cells were delicately re-suspended in sterile PBS, ensuring viability[29]. A portion of 500 µL bacterial suspension at a concentration of 10^6 CFU/mL was then transferred to a sterile Petri dish with a diameter of 100 mm. The Petri dish was placed inside the plasma sterilization chamber and its lid was opened. The bacterial suspension was then exposed to a controlled atmosphere of air and ozone plasma at 0.3–0.5 mbar pressure and about 1 kW power. The exposure time was varied from 30, 60, 180 and 300 s for to assess its effect on the bacterial population. Following the plasma treatment, the suspension was transferred to sterile tubes containing 5 mL of sterile PBS. Additionally, for the purpose of comparison, a control was prepared by directly adding 500 µL of the bacterial suspension (10^6 CFU/mL) to 5 mL sterile PBS.

Enumeration of bacterial colony

To determine bacterial viability post-treatment, serial dilutions (10^{-1} to 10^{-6}) of each treated bacterial sample were prepared in sterile PBS. From each dilution, 0.1 mL was spread onto separate nutrient agar plates using a sterile glass spreader. These plates were then incubated at 37 °C for 24 h, allowing the growth of bacterial colonies. Colonies were manually counted, and CFU/mL values were calculated using the formula[29,36],

$$CFU/mL = \frac{Number\ of\ colonies \times Dilution\ factor}{Volume\ of\ sample\ plated\ (mL)}$$

Afterwards, logarithmic reduction in bacterial population was determined using the following formula[3],

$$Log\ reduction = log_{10}\left(\frac{N_0}{N}\right)$$

where, N_0 = Initial bacterial count before plasma treatment (CFU/mL). N = Bacterial count after plasma treatment (CFU/mL).

The remaining stock of plasma-treated bacterial samples were stored at 4 °C, preserving them for further detailed spectroscopic and microscopic analyses. The plasma-treated bacterial samples were stored at 4 °C to prevent any further metabolic activity and growth. Also, all samples were processed for further critical analysis within 24 h of treatment to minimize any potential effects related to storage. Therefore, the effect of low-temperature storage on our results is considered negligible[37].

Measurement of reactive oxygen species (ROS)

The investigation focused on assessing the production of ROS such as, hydroxyl radicals ($^{\cdot}OH$) and hydrogen peroxide (H_2O_2) on the bacterial membrane pre- and post-plasma treatment across varying treatment durations for both *S. aureus* and *S. abony*. Terephthalic acid (TA) and Dichlorodihydrofluorescein Diacetate (DCFH-DA) non-fluorescent probes were employed as specific markers for the detection of $^{\cdot}OH$ and H_2O_2 radicals, respectively[29]. Following plasma treatment, these probes were introduced into the bacterial suspension and allowed to incubate under dark conditions at room temperature for a duration of 30 min. Subsequently, fluorescence intensities corresponding to the presence of terephthalic acid (excitation wavelength of 315 nm and emission wavelength of 415 nm) and DCFH-DA (excitation wavelength of 488 nm and emission wavelength of 525 nm) were measured. The recording of fluorescence spectrum was done under ambient conditions using an FP-6500 Jasco Spectrofluorometer.

Confocal laser scanning microscopy (CSLM)

In a distinct experiment, 1 mL of bacterial cell suspension was subjected to plasma exposure for durations of 0, 30, 60, 180, and 300 s. Following plasma exposure, 5 µL of PI solution was introduced into each bacterial sample, and the mixtures were incubated at room temperature in darkness for 30 min. Subsequently, the stained cells underwent washing and were re-suspended in sterile PBS. These bacterial samples were then mounted onto glass slides and visualized under confocal microscopy (Leica TCS SP8) utilizing an oil immersion objective to examine red fluorescent dead cells after different plasma exposure time[38].

Fluorescence-activated cell sorting (FACS)

FACS analysis using propidium iodide (PI) staining is an effective technique to evaluate cell viability. PI is a fluorescent dye that binds to DNA, but it can only enter cells with compromised membranes, typically those that are dead or dying. This information is useful for understanding cellular responses to plasma treatments. For the analysis, 1 mL samples of both untreated (control) and plasma-treated (30, 60, 180, and 300 s) bacterial cell suspensions were prepared, with an additional unstained control sample. To initiate PI staining, 3 µL of a 5 mM PI solution was added to each tube, followed by gentle vortexing to mix. The tubes were then incubated in the dark for 10 min at 28 °C before flow cytometry measurements. The stained samples were analyzed on a BD FACS Aria flow cytometer with a 488 nm excitation source and a 616/23 bandpass emission filter for PI. According to

BD specifications, PI fluorescence was detected within the PE/Texas Red filter, and dot plots were recorded for analysis[39,40].

Field emission scanning electron microscopic (FE-SEM) imaging

The bacterial samples subjected to plasma exposure alongside the control were gathered and prepared for observation under FE-SEM. The cell fixation procedure involved a sequential treatment regimen, initially immersing the specimens in 2.5% glutaraldehyde for 2 h, followed by a fixation in 1% osmium tetroxide for 1 h at 4 °C, with subsequent rinsing in distilled water. Dehydration ensued through a graded ethanol series (50%, 60%, 70%, 80%, and 90% (*v*/*v*) ethanol) with sequential immersion for 5 min in each solution to gradually remove the water content from the sample. The final dehydration step was performed in absolute ethanol (100%) for 10 min to ensure complete dehydration[41]. The dehydrated samples were then subjected to air drying to prevent structural collapse before SEM imaging. Finally, dehydrated samples were affixed onto a silicon wafer and coated with gold ions for 2 min via a sputtering apparatus (JEOL JFC-1600 auto fine coater) to render them conductive. Examination was performed employing FE-SEM (JEOL JSM-7600F) with a secondary electron (SE) detector, operating at a voltage of 5.0 kV. Morphological variations induced in the bacterial population by various durations of exposure to air and ozone plasma were analyzed and documented through SEM micrography[29].

Measurement of bacterial membrane potential

The membrane potential (MP) in *S. aureus* and *S. abony* have been measured using voltage-sensitive, 3,3′-Diethyloxacarbocyanine iodide [$DiOC_2(3)$] fluorescent dye (excitation wavelength 483 nm and emission wavelength 503 nm)[42]. After the plasma treatment, 10 µL of 50 µM $DiOC_2(3)$ solution was added to the control and treated bacterial suspension and permitted to incubate in darkness at room temperature for a period of 30 min. The fluorescence spectrum was recorded using an RF 6000 Shimadzu Spectrofluorophotometer under room temperature[39]. The purpose of using $DiOC_2(3)$ in bacterial membrane potential assays is to assess the integrity and functionality of the bacterial cell membrane, specifically its electrical potential ($\Delta\psi$), which is a key indicator of cellular viability and metabolic state.

DNA leakage study

The study on the leakage of double-stranded (ds) DNA following plasma treatment was carried out by evaluating the ultraviolet (UV) absorption at 260 nm for each bacterial sample[29,43]. Spectral data were obtained for the wavelength range of 200–400 nm using UV Vis-Spectrophotometer (Shimadzu UV-61 double beam spectrophotometer) with a 50 µL sample quartz cuvette, without storing the treated cell suspension. Before recording the spectra, baseline correction was performed using PBS as a reference solution.

Attenuated total reflectance fourier transform infrared spectroscopy (ATR-FTIR)

The infrared (IR) spectra of each plasma treated bacterial sample (0, 30, 60,180 and 300 s) were acquired to examine their molecular conformation. The plasma-treated suspension underwent gentle mixing using a rotary shaker, and a 5 µL aliquot was transferred onto a single bounce ATR diamond crystal. Prior to spectral measurement, spectral subtraction employing PBS was conducted. Subsequently, the IR spectra were recorded in ATR mode of FTIR spectroscope (PerkinElmer L1600300 TwoLiTa) and Spectrum software. Spectral data were collected within the wavenumber range of 900–4000 cm^{-1}, with a scanning velocity of 0.2 cm/s and a spectral resolution of 4 cm^{-1}[29,43].

Statistical analysis

The experiments were carried out in triplicate (n = 3). Following data collection, the mean and standard deviation values were incorporated into the graphical representations. Origin software (OriginLab Inc.) was used for graph plotting. Statistical difference between the groups were performed using one-way analysis of variance (ANOVA) with a significance level set at $p < 0.05$, followed by two-sample t-tests, also with a significance level of $p < 0.05$, utilizing Microsoft Office Excel software.

Results and discussions

Non-thermal microwave plasma optical characterization

Figure 2 illustrates the optical emission spectrum spanning the wavelength range of 300–1000 nm, characterizing air (0.8%) and ozone (99.2%) plasma generated via a microwave source, operating at an sub-atmospheric pressure range of 0.3–0.5 mbar and input microwave power of about 1 kW. The spectrum were recorded with an acquisition time of 500 ms *per* scan, averaging over five scans for each measurement. The nature and concentration of the plasma species generation depends on the type of plasma source used and the composition of injected gas[44]. The emitted wavelengths are identified using established spectral line databases, which lists wavelengths associated with specific atomic and molecular transitions in plasma the atomic emission line of nitrogen are observed at 340.45 nm, 365 nm, and 396.12 nm. The appearance of hydrogen Balmer transition lines such as, $H_\alpha = 656$ nm, $H_\beta = 481$ nm and $H_\gamma = 435.41$ nm indicate the presence of hydrogen comprising species mainly stable and long lived peroxide (H_2O_2)[45].The hydroxyl radicals ($^{\cdot}OH$) at 320 nm and other oxygen species appeared at 398 nm (O II), 510 nm (O III) and 705 nm (O IV)[29]. The $^{\cdot}OH$ radical is produced by the reaction of oxygen atom with H_2O molecule. The occurrence of these reactive species induces various cytotoxic and genotoxic effects, resulting in cellular damage, as discussed in later sections[46].

Logarithmic CFU/mL reduction analysis

The colony count assay (CFU/mL) served as quantitative measure of viable and culturable bacterial colonies before and after plasma treatment, providing evidence of the effectiveness of microwave plasma in reducing

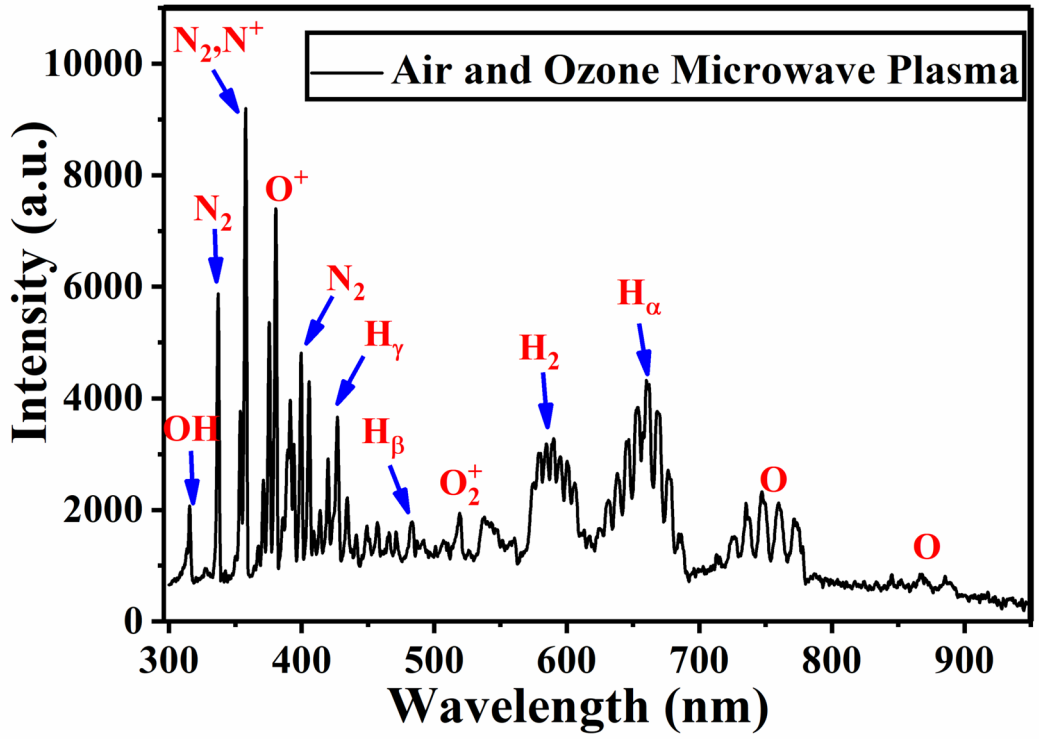

Fig. 2. Optical emission spectral analysis of air-ozone microwave plasma with spectra recorded in the wavelength range of 300–1000 nm.

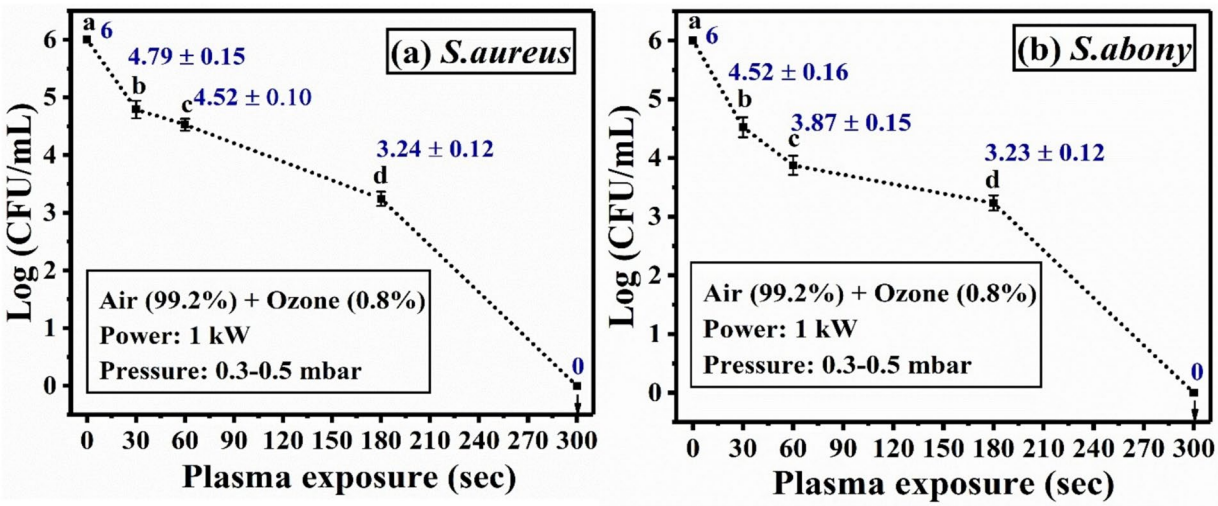

Fig. 3. The reduction curves showing a 6 Log (CFU/mL) decrease for (**a**) *S. aureus* and (**b**) *S. abony* are presented. Lowercase letters are used to denote statistically significant differences ($p < 0.05$, n = 3) between treatment times.

culturable bacterial populations. As shown in Fig. 3a,b, a progressive and significant reduction ($p < 0.05$) in log (CFU/mL) was observed with increasing plasma exposure time for both *S. aureus* and *S. abony*. After 300 s of plasma exposure, no viable colonies were detected for both *S. aureus* and *S. abony* in the CFU assay.

Mai-Prochnow et al. showed correlation between cold atmospheric plasma led inactivation of bacteria and composition of cell wall structures. They have demonstrated that Gram negative species with a thinner cell wall are inactivated more rapidly than Gram positive bacteria with a thicker cell wall[47]. In our study, the reduction curves from Fig. 3 suggests a trend where Gram negative *S. abony* appears to show a relatively rapid log (CFU/mL) reduction compared to Gram positive *S. aureus*, particularly during the early exposure periods (30 and 60 s). For example, at 60 s of plasma exposure, *S. aureus* showed a 4.5-log, while *S. abony* showed a 3.8-log

reduction. However, this observation is based on qualitative analysis. We speculate that, this slight difference can be attributed to structural and compositional differences in their cell walls, outer membrane properties, and charge distributions which influences plasma-induced damage at a molecular level[48]. A study by Montie et al. has suggested that the Gram negative bacterial cell allows ROS to penetrate by diffusion, and cell membranes are vulnerable to atmospheric glow discharge plasma[49]. We also speculate that, Gram-negative *S. abony* has a thinner peptidoglycan layer and an outer membrane made of lipopolysaccharides (LPS), which plays a main role in its plasma susceptibility[47,50]. Their outer membrane with porins facilitate the diffusion of reactive plasma generated species towards the cytoplasmic membrane making them more vulnerable leading to fast cell damage in the initial point[47,49,51].

In contrast, Gram-positive *S. aureus* has a thicker, highly cross-linked peptidoglycan layer, which can act as a physical barrier, delaying the diffusion of reactive species and resulting in a more gradual inactivation process[49,52]. Moreover, Gram-positive *S. aureus* have a negative charge due to the presence of teichoic acids in the thick peptidoglycan cell wall and the outer membrane of Gram-negative *S. abony* also has highly negatively charged LPS, but neutral reactive plasma species can diffuse through both bacterial cell walls without being repelled by electrostatic forces[47,53,54]. However, after prolonged exposure (≥ 180 s), both bacterial strains showed similar inactivation rates (3.2 log reduction), signifying that increased plasma treatment effectively neutralizes structural differences.

Over-production of reactive oxygen species

Fluorescence spectroscopy is employed to measure the levels of reactive species, including hydroxyl radicals ($^{\cdot}OH$) and non-radical hydrogen peroxide (H_2O_2), detected in the bacterial sample exposed to plasma. As shown in the OES spectral analysis, these species generated in the plasma diffuse inside the bacterial membrane during exposure. In presence of plasma, ozone (O_3) significantly contributes to the generation of these reactive species. The following major reactions involved in $^{\cdot}OH$ and H_2O_2 production in ozone-assisted plasma sterilization[55]:

(i) *Dissociation of O_2*:

$$O_3 + e^- \rightarrow O_2 + O^{\cdot} + e^-$$

(ii) *$^{\cdot}OH$ Production:*

$$O^{\cdot} + H_2O \rightarrow 2^{\cdot}OH$$
$$e^- + H_2O \rightarrow {}^{\cdot}OH + H^{\cdot} + e^-$$

(iii) *H_2O_2 Formation:*

$$^{\cdot}OH + {}^{\cdot}OH \rightarrow H_2O_2$$
$$O_3 + H_2O \rightarrow H_2O_2 + O_2$$

(iv) *Amplification of ROS through Fenton and Haber–Weiss Reactions*

During plasma sterilization, the interaction between plasma-generated external reactive species and bacterial cells can enhance the levels of reactive species already present within the cells. Once inside the cell, plasma-generated H_2O_2 and superoxide (O_2^-) can participate in Fenton and Haber–Weiss reactions with intracellular iron ions (Fe^{2+}) to produce $^{\cdot}OH$, the most damaging ROS for cellular components:

$$H_2O_2 + Fe^{2+} \rightarrow {}^{\cdot}OH + OH^- + Fe^{3+}$$

This reaction significantly amplifies the amount of ROS within the cell, leading to more severe oxidative damage to cellular structures[54,56].

In order to validate and quantify the presence of $^{\cdot}OH$ radicals bound to the membrane, bacterial cells underwent staining with a non-fluorescent TA probe subsequent to plasma treatment. Then, the fluorescence spectra of each bacterial sample were recorded. TA molecules serve as reliable scavengers specifically for $^{\cdot}OH$, with no propensity for reacting with other oxygen radical species such as H_2O_2, O_2, and HO_2. The binding of TA molecules with $^{\cdot}OH$ yields the oxidation product, 2-hydroxy terephthalic acid (HTA), which emits fluorescence. This characteristic enables the detection and qualitative evaluation of hydroxyl radicals[29,57]. Likewise, for the detection of H_2O_2, the widely recognized DCFH-DA probe was utilized. This probe, permeable to cells, undergoes efficient hydrolysis by esterase within the cellular matrix, forming DCFH, which remains sequestered within the cell. The interaction of H_2O_2 with DCFH leads to the production of a fluorescent derivative, dichlorofluorescein (DCF), whose levels can be assessed using fluorescence measurement techniques.

The graphs depicted in Fig. 4a,b demonstrate the generation of long-lasting H_2O_2, assessed using the DCFH-DA probe. Similarly, Fig. 4c,d illustrate the fluorescence spectra acquired using the TA probe, aimed at detecting the presence of $^{\cdot}OH$ radicals on the bacterial membranes of *S. aureus* and *S. abony*, respectively. The fluorescence spectra exhibits a progressive augmentation at 525 nm and 415 nm with prolonged plasma exposure, indicative of an escalating concentration of H_2O_2 and $^{\cdot}OH$ radicals respectively. The production of these radicals induces oxidative stress within the bacterial cell's internal milieu, ultimately leading to cell death or inactivation[54].

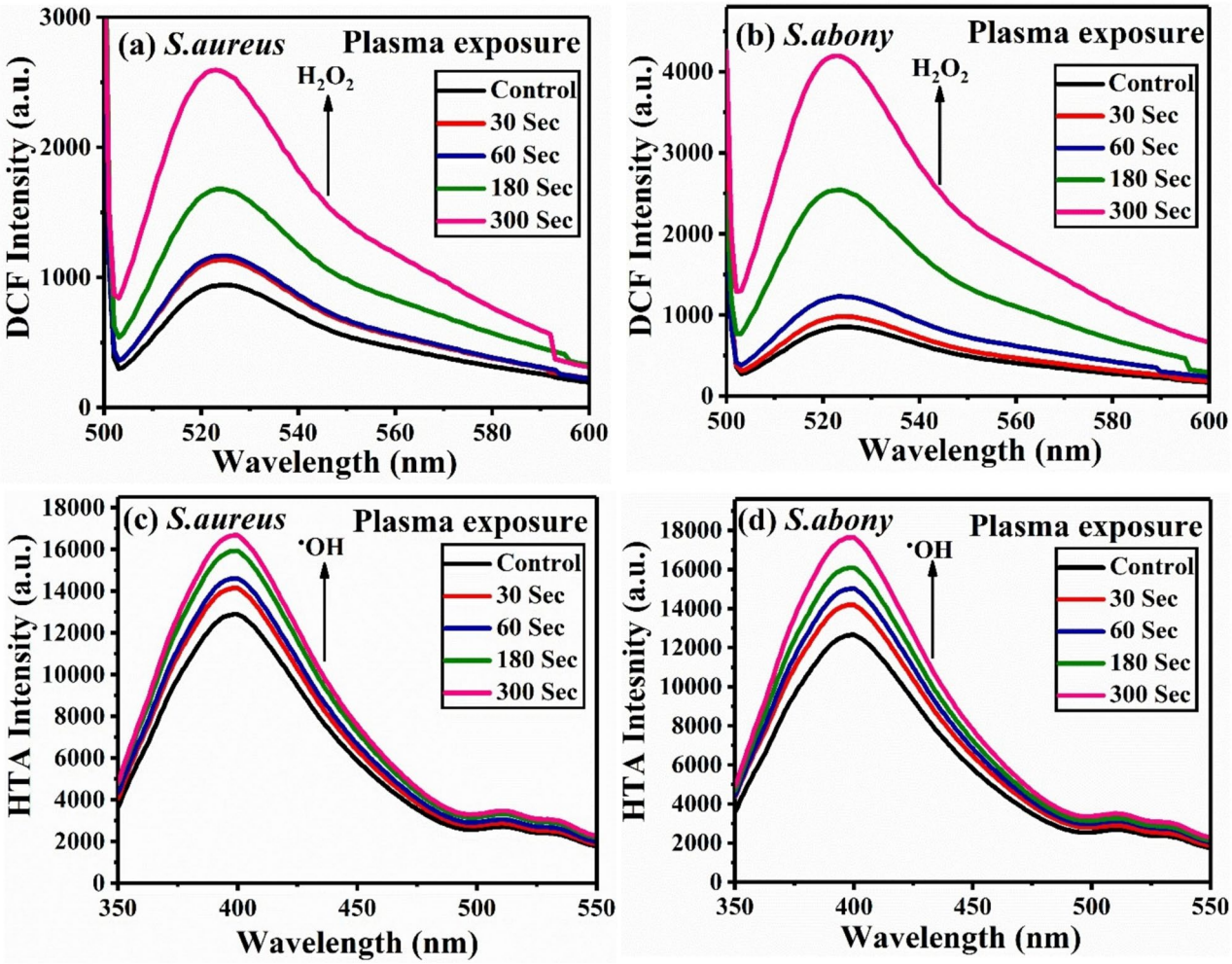

Fig. 4. The fluorescence spectra of *S. aureus* and *S. abony* treated with plasma reveal an excessive generation of hydrogen peroxide (H_2O_2) in (**a**) and (**b**), and hydroxyl radicals ($^{\cdot}OH$) in (**c**) and (**d**), respectively.

Further, quantitative analysis of H_2O_2 and $^{\cdot}OH$ production, as depicted in Fig. 5a,b, reveals a time-dependent elevation in the percentage (%) change (with respect to control sample) of reactive radicals following plasma exposure. The increase in fluorescence intensities of treated bacterial samples was calculated at wavelengths corresponding to peak intensity, utilizing the % change formula.

In Fig. 5a, it was observed that following 300 s of plasma treatment, *S. aureus* displayed a significant increase of 173.27% and 30.30% in H_2O_2 and $^{\cdot}OH$ radicals, respectively. Similarly, as illustrated in Fig. 5b, a substantial rise ($p < 0.05$) of 391.84% and 40.13% in H_2O_2 and $^{\cdot}OH$ radicals, respectively, was recorded in *S. abony* following the same duration of plasma treatment. Particularly noteworthy was the elevation in the proportion of long-lived H_2O_2 in both bacteria. The extended longevity of more stable H_2O_2 radicals, facilitated by the cell structure providing suitable binding sites, resulted in higher production compared to $^{\cdot}OH$ radicals in both bacterial strains. H_2O_2 can persist in both extracellular and intracellular environments, allowing it to accumulate more easily within bacterial cells during and after plasma treatment. The prevalence of short-lived $^{\cdot}OH$ radicals over H_2O_2 can be attributed to their heightened reactivity. Notably, the enhanced and rapid diffusion of H_2O_2 and $^{\cdot}OH$ radicals into the Gram-negative *S. abony*, facilitated by the presence of porins on the outer cell membrane, led to swift bacterial inactivation[51,58]. This observation is corroborated by the CFU count data, which indicates reduced colony formation, suggesting faster inactivation of *S. abony* compared to *S. aureus*. Additionally, the subsequent sections detailing plasma-mediated antibacterial analysis utilizing confocal imaging, flow cytometry, ATR-FTIR and UV–visible methods further validate the present data.

Confocal imaging for analyse dead cells

To delve deeper into the mechanisms underlying plasma-induced damage to cell membranes, we can employ the count of red fluorescent cells as a practical indicator of bacterial cell damage through single staining with propidium iodide (PI), which binds to DNA of dead cells in the medium[59]. PI, a large molecule, cannot pass through intact cell membranes but can permeate damaged membranes of deceased or dying cells, aiding in the assessment of dead cell proportions within a sample. Figures 6a and 7a represent the *S. aureus* and *S. abony* samples, respectively, which were not treated with plasma, showing no evidence of dead cells in the control

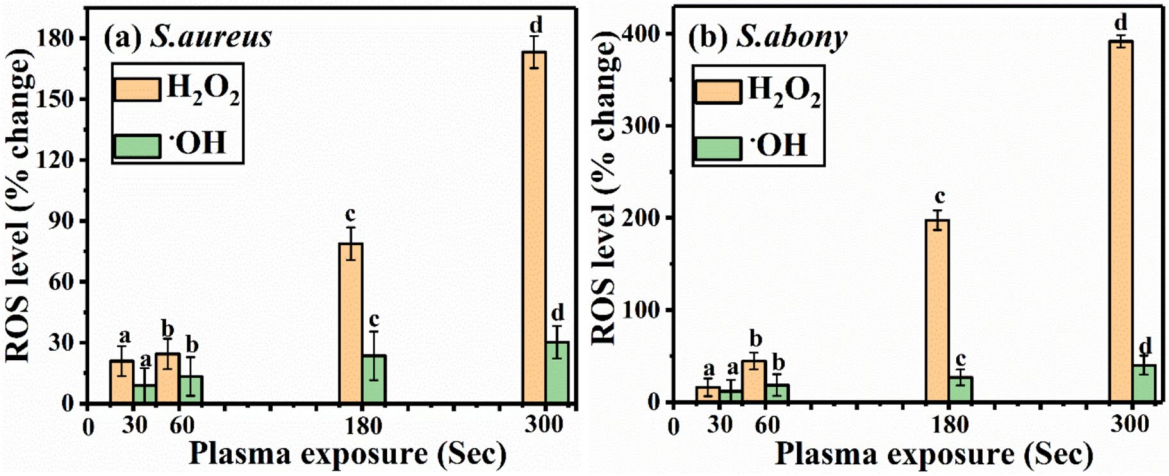

Fig. 5. Quantitative analysis depicting the percentage increase in H_2O_2 and $^{\cdot}OH$ production on the bacterial membranes of (**a**) *S. aureus* and (**b**) *S. abony* after exposure to plasma at different time intervals. A significant elevation in ROS levels ($p < 0.05$, n = 3) was observed compared to the control.

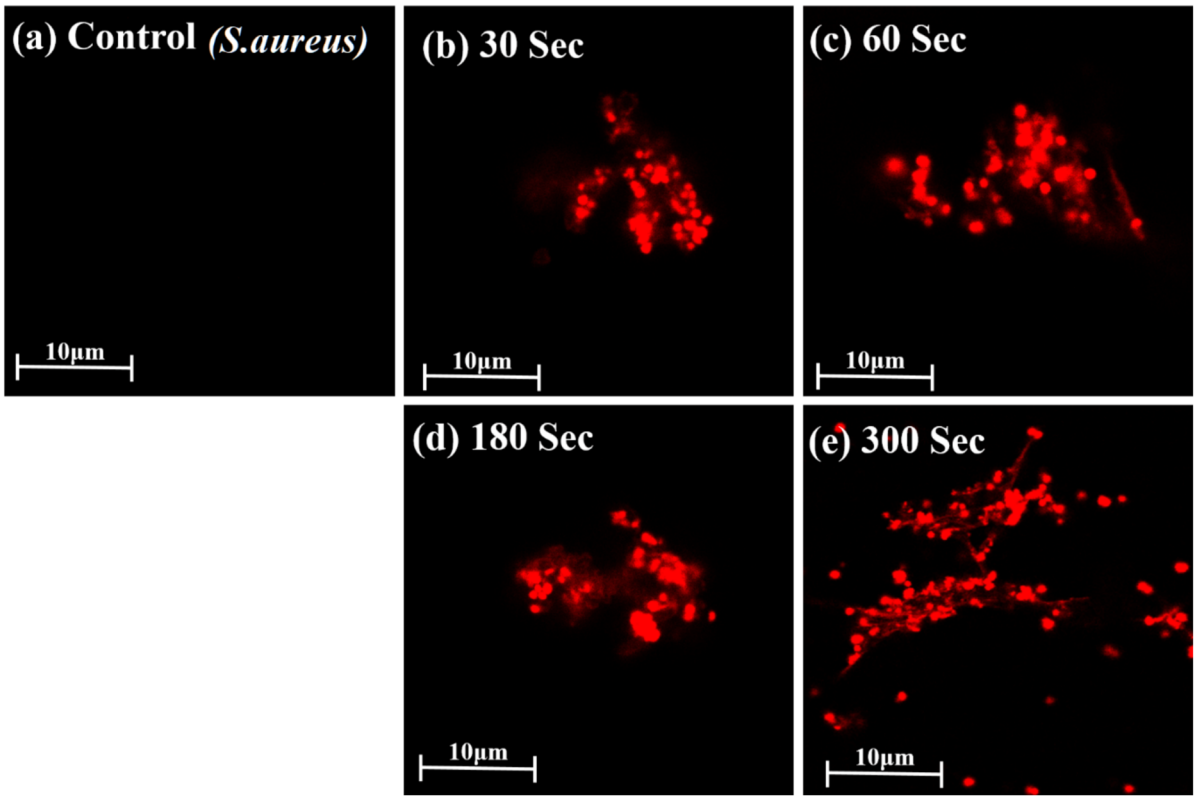

Fig. 6. *S. aureus* were exposed to plasma for (**a**) 0 s (**b**) 30 s (**c**) 60 s (**d**) 180 s (**e**) 300 s and stained using propidium iodide. Images were taken using confocal microscope showing red fluorescent dead bacteria (PI penetration).

images. Plasma-treated *S. aureus* and *S. abony*, as depicted in Figs. 6b–e and 7b–e respectively, exhibit clusters of dead fluorescent cells. The results of CFU assay reflects overall viability and culturability captured by log (CFU/mL) reduction trends, while PI staining shows membrane permeability. The higher accumulation of PI in *S. aureus* compared to *S. abony* after plasma treatment was observed in Fig. 6b–e due to differences in their outer cell wall structures and membrane compositions. In case of *S. aureus*, thick peptidoglycan layer, which can act as a mesh-like structure that may retains PI more, indicates greater membrane damage but not direct viability[60]. Whereas, Gram-negative bacteria show more scattered fluorescence in the microscopy images, indicating that the

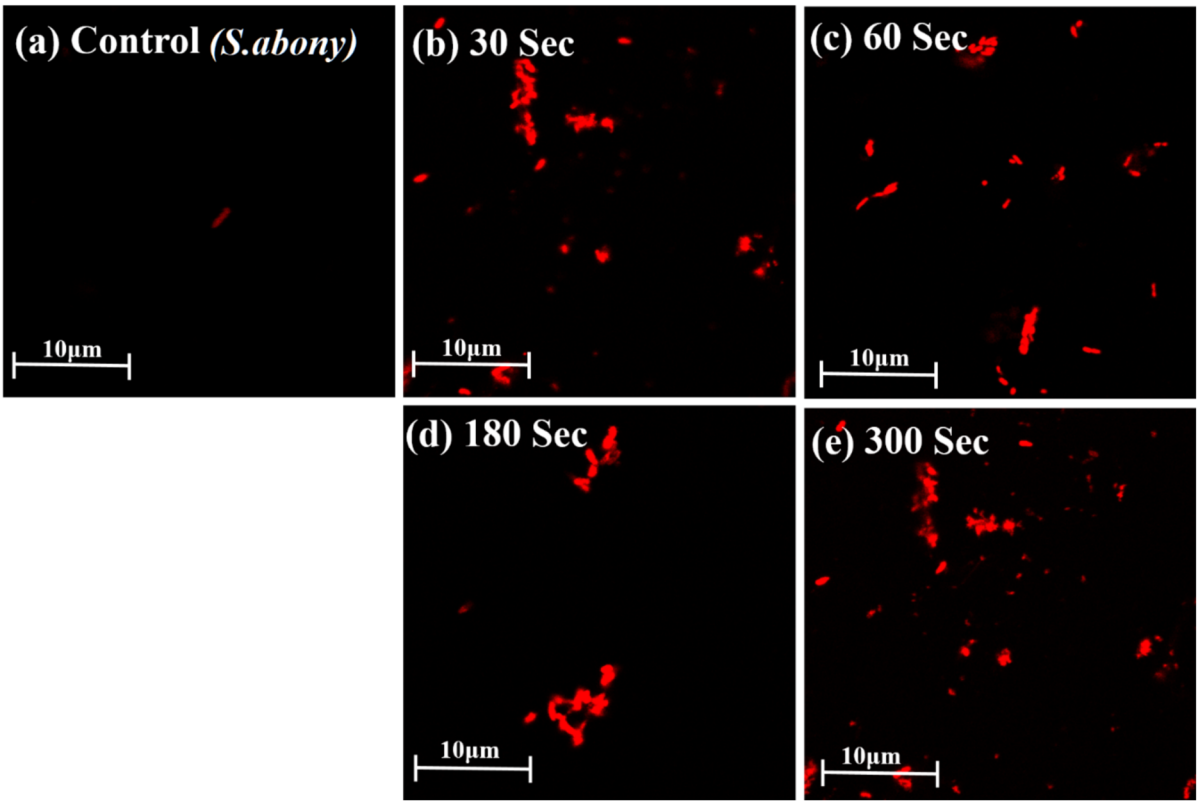

Fig. 7. *S. abony* were exposed to plasma for (**a**) 0 s (**b**) 30 s (**c**) 60 s (**d**) 180 s (**e**) 300 s and stained using propidium iodide. Images were taken using confocal microscope showing red fluorescent dead bacteria (PI penetration).

PI dye penetrates less uniformly. *S. abony* possess an outer membrane composed of lipopolysaccharides, which can be more susceptible to quick disruption, potentially leading to quicker leakage of intracellular contents, including PI and hydrophobic region of this lipopolysaccharides may prevent PI from freely diffusing into cells. However, the presence of porins and a compromised outer membrane due to plasma allows inconsistent PI penetration and binding to DNA leading to fluorescence[61,62].

Additionally, the current study presents FE-SEM images of Gram-negative bacteria that reveal cell expansion following plasma treatment, which may account for the observed reduction in cell aggregation. As plasma treatment duration increases, the quantity of fluorescent cells of *S. aureus* and *S. abony* gradually rises, along with a corresponding increase in the count of inactivated bacteria, signifying a positive correlation between fluorescent red cell count and bacterial inactivation. This implies that heightened cell membrane permeability corresponds to more severe membrane damage. Dolezalova et al. employed PI staining in experiments to validate plasma-induced damage to *E. coli* cell membranes[63]. Lv Xiaoye et al. also found increased permeability of PI in *Salmonella typhimurium* cell membrane after exposed to DBD cold plasma at different time intervals using confocal microscopy and discussed similar effect of plasma on cell membrane[38]. Therefore, it can be inferred that plasma-induced oxidation and damage to the cell membrane increase membrane permeability. This study also provide insights into how structural differences between both bacteria influence PI uptake and retention under conditions of compromised membrane integrity.

Analysis of cell viability using FACS

The flow cytometric analysis of dead bacterial cell counts following plasma treatment with propidium iodide dye staining revealed a notable trend, as illustrated in Figs. 8a–e and 9a–e for *S. aureus* and *S. abony*, respectively. The scatter plots depict side scatter (SSC-A) versus forward scatter (FSC-A) area, with gating performed to identify the percentage of dead cell (PI-positive) sub-population and distinguish PI-negative (intact) cells. Since dead cells have compromised membranes, they take up PI and emit fluorescence when excited by a laser during FACS analysis. In both treated bacterial samples, differences in the gates with PI-positive cells may result from variations in plasma treatment time or staining. As exposure time increases, the proportion of cells taking up PI increases, leading to a gradual shift in fluorescence intensity rather than a fixed threshold for all samples[64].

Sharkey et al. analyzed the effect of atmospheric pressure plasma jets (APPJs) on *E.coli* cells and also used propidium iodide single dye staining for assessment of membrane damage using flow cytometry[65]. After 10 min of PI uptake by the dead cells, dot plot were recorded following plasma treatment. With increasing plasma treatment duration, the number of aggregated dead cells also increased, indicating a direct correlation between

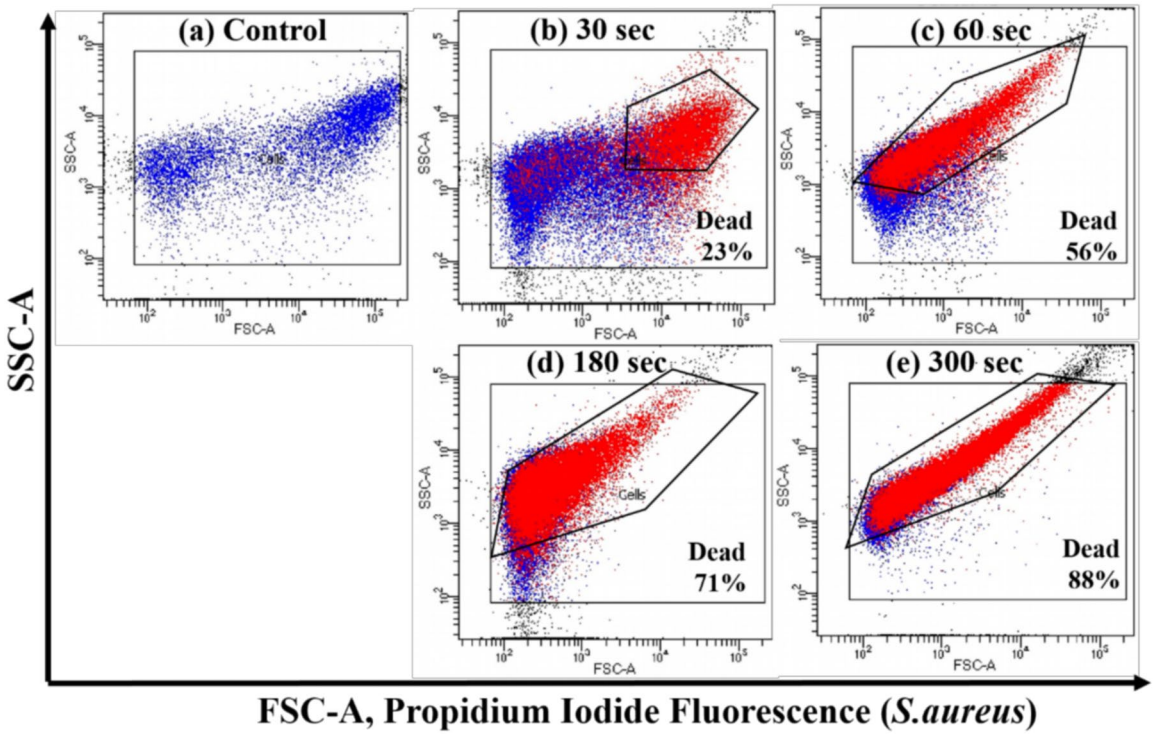

Fig. 8. Fluorescence dot plots represents plasma treated *S. aureus* cells (**a**) Control (**b**) 30 s (**c**) 60 s (**d**) 180 s, and (**e**) 300 s, analysed via FACS represented gated dead cells sub-population. Cells stained with PI (red colour), indicating membrane damage caused by plasma exposure.

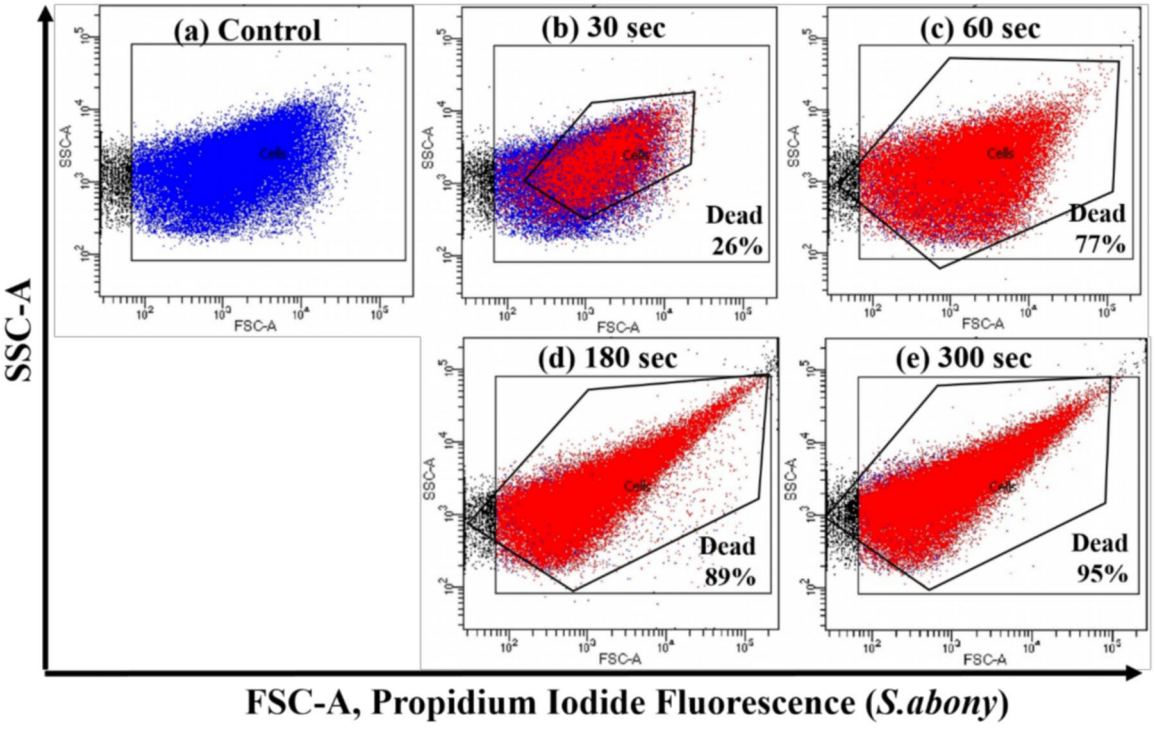

Fig. 9. Fluorescence dot plots represents plasma treated *S. abony* cells (**a**) Control (**b**) 30 s (**c**) 60 s (**d**) 180 s, and (**e**) 300 s, analysed via FACS represented gated dead cells sub-population. Cells stained with PI (red colour), indicating membrane damage caused by plasma exposure.

plasma treatment time and bacterial cell death. We can correlate these findings with confocal images due to the application of a similar propidium iodide staining method, which selectively binds to impaired or dead cells.

The results obtained from microbiological seeding and flow cytometry are correlated. The CFU assay demonstrated a progressive decline in log (CFU/mL) with increasing plasma exposure times, with inactivation observed after 300 s. Similarly, flow cytometry data revealed an increasing proportion of PI-stained dead cells, reaching 88% for *S. aureus* and 95% for *S. abony* after 300 s of exposure shown in Figs. 8e and 9e, respectively. These findings confirm that microwave plasma effectively compromises bacterial membrane integrity, leading to cell death. The 12% of *S. aureus* and 5% of *S. abony* cells may remained in the viable but non-culturable (VBNC) or sub-lethally injured state of bacteria detected in flow cytometry[63,66]. The slight discrepancies between the CFU and flow cytometry results can be attributed to the presence of VBNC cells that retain metabolic activity but fail to proliferate under standard culturing conditions[67]. Flow cytometry was used to complement microbiological seeding by providing a quantitative and real-time analysis of bacterial membrane damage. After plasma treatment, CFU analysis requires an incubation period of 24 h. Whereas flow cytometry allows for instant evaluation of bacterial viability and injured or dead cell counts. By combining these two methods, comprehensive understanding can be established for the plasma-induced bacterial inactivation mechanism which strengthens the reliability of our findings.

The variance in the mortality rate for both bacterial classes under equivalent plasma exposure durations can be attributed to differences in cell wall composition and membrane permeability between Gram-positive and Gram-negative bacteria. The thinner layers of peptidoglycan in the cell wall of Gram-negative bacteria make them more susceptible to plasma compared to the thicker layers found in Gram-positive bacteria. When the outer membrane of *S. abony* is impaired rapidly due to the diffusion of plasma-generated reactive species, stress is created, subsequently allowing propidium iodide molecules to bind with released or leaked nucleic acids from dead cells in suspension, thus increasing the fluorescence signal.

Microwave plasma induced bacterial morphological changes

The surface morphological characteristics of both *S. aureus* and *S. abony* were investigated before and after plasma treatment, as illustrated in Figs. 10a–e and 11a–e correspondingly. Figure 10a depicts the morphology of untreated *S. aureus*, characterized by regularly round-shaped cells with smooth surfaces. Upon exposure to plasma, a notable aggregation of cells occurred, followed by the initiation of membrane rupture after 30 s. Prolonged exposure to plasma resulted in increasingly severe cellular damage. The oxidative stress induced by plasma treatment prompted the formation of cup-shaped morphologies, wherein the cell membrane exhibited inward curvature, forming distinctive cup-shaped structures[68]. This alteration in morphology is likely a consequence of localized membrane damage, leading to changes in both permeability and structural integrity, along with the concurrent destruction of the thick cell wall typical of Gram-positive bacteria. The compromised cell walls of plasma-treated bacteria were unable to uphold cellular structural integrity, ultimately leading to cell lysis. Consequently, the release of cellular contents such as cytoplasm, nucleic acids, and proteins ensued, disrupting cellular metabolism and ultimately resulting in cell death[69].

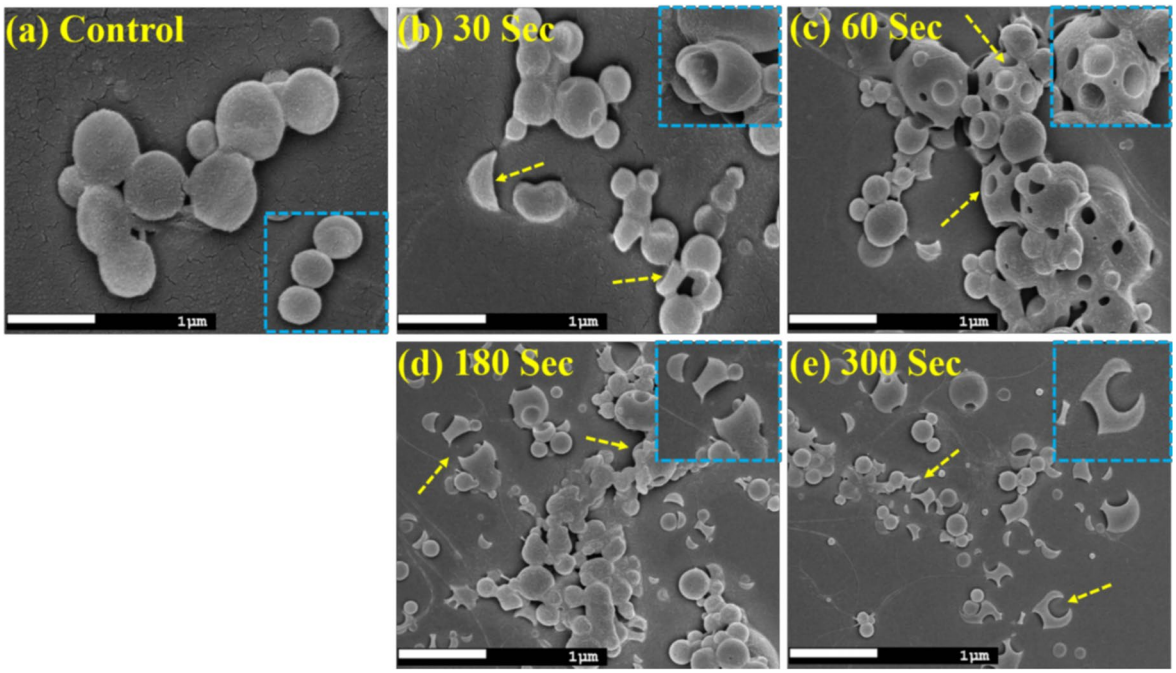

Fig. 10. FE-SEM micrographs illustrate the surface morphologies of *S. aureus* for (**a**) control (untreated), plasma treatment for (**b**) 30 s, (**c**) 60 s, (**d**) 180 s, and (**e**) 300 s.

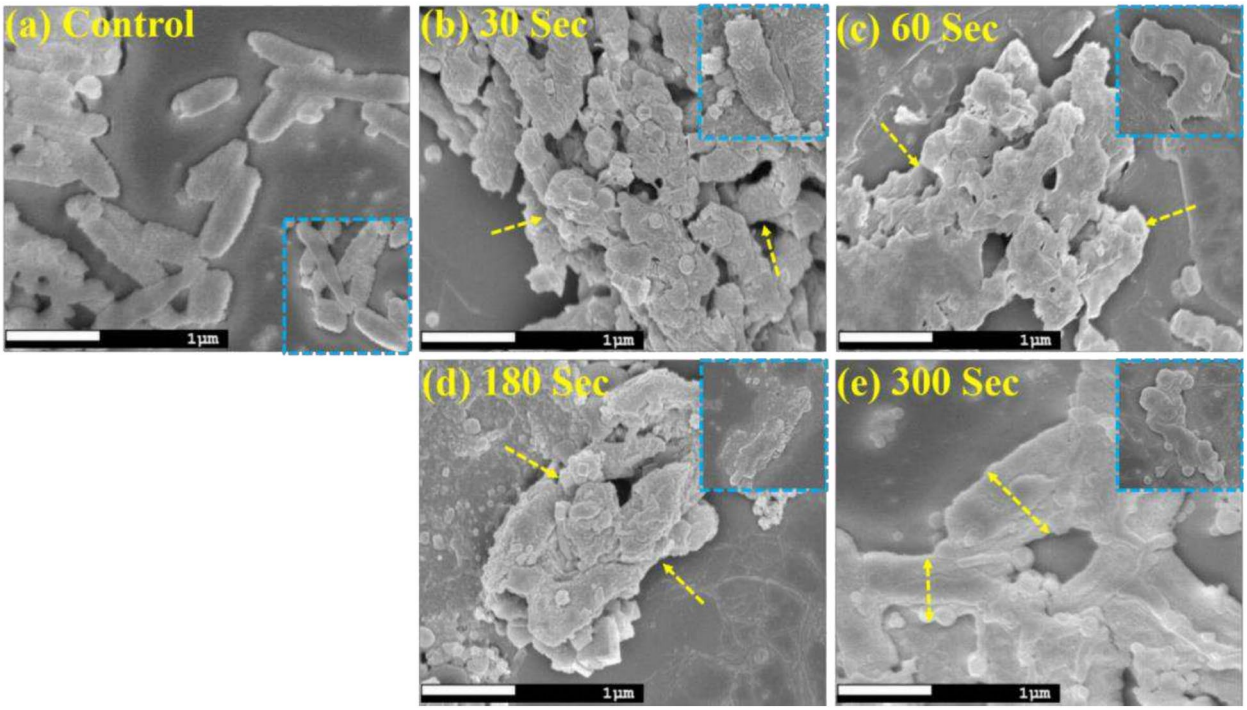

Fig. 11. FE-SEM micrographs illustrate the surface morphologies of *S. abony* for (**a**) control (untreated), plasma treatment for (**b**) 30 s, (**c**) 60 s, (**d**) 180 s, and (**e**) 300 s.

Figure 11a depicts the untreated FE-SEM image of the Gram-negative *S. abony*. Upon exposure to plasma which is shown in Fig. 11b–e, the regularly rod-shaped bacteria underwent a transformation into irregular shapes, dented, and wrinkled, with noticeable increases in surface roughness apparent after 30 s of treatment. The outer membrane is compromised due to oxidative stress caused by reactive molecules passing through porins, the bacteria experience structural changes and cellular expansion. Subsequently, cellular expansion ensued, resulting in bacterial swelling. The aggregated cells exhibited compromised membrane integrity, which facilitated the leakage of intracellular material present in *S. abony*[70].

Analysis of membrane potential (MP) using $DiOC_2(3)$

The membrane potential serves as a pivotal factor in numerous critical physiological processes within bacterial organisms. To assess relative membrane potentials in bacteria, fluorescent probes have been extensively employed. In this study, $DiOC_2(3)$, a cationic carbocyanine and voltage-sensitive dye, was utilized to gauge the relative membrane potentials of bacteria subsequent to exposure to plasma treatment[71].

$DiOC_2(3)$ is a positively charged fluorescent dye that either accumulates intracellularly or extracellularly in a manner contingent upon voltage, which can be monitored through fluorescence intensities. Spectral analysis of fluorescence emitted by $DiOC_2(3)$-stained bacterial samples, exposed to plasma (0, 30, 60, 180, and 500 s), was conducted at an emission wavelength of 503 nm using a spectrofluorophotometer depicted in Fig. 12a,b. Increased fluorescence intensities were observed consequent to alterations in the membrane potential of cells post-plasma treatment in comparison to the control. The dye exhibited greater fluorescence intensity in both *S. aureus* and *S. abony*, indicative of membrane depolarization, resulting in a gradual blue shift (lower wavelength) in the fluorescence emission spectrum observed in treated bacterial samples[39]. Upon depolarization, $DiOC_2(3)$ can penetrate the cell and vividly stain the cellular membranes. Typically, in healthy cells, dye becomes more concentrated in intact membranes maintaining a membrane potential, prompting dye self-association[71].

Figure 12c,d illustrates the changes in bacterial membrane potential ($p < 0.05$) subsequent to plasma treatment relative to the resting membrane potential of control bacterial samples. The fluorescence intensities, converted into percentage increase in fluorescence intensity (%), signify a change in membrane potential. This variation in membrane potential entails the movement of the cell's resting membrane potential towards zero, inducing a more positive state, hence depolarizing the membrane. Consequently, the electrical charge disparity between the intracellular and extracellular environment reduces. Also, this study presents new findings indicating that microwave plasma treatment impacts bacterial cells through electrophysiological effects, such as membrane potential disturbance and depolarization, which contribute to membrane damage, as demonstrated by spectrofluorometric analysis[72].

Microwave plasma-induced hyperchromicity of DNA

The nucleic acid found within DNA molecules exhibits strong absorption of light at 260 nm, detectable through UV absorbance spectroscopy. In Fig. 13a,b, the absorption peak at 260 nm increases in relation to the duration

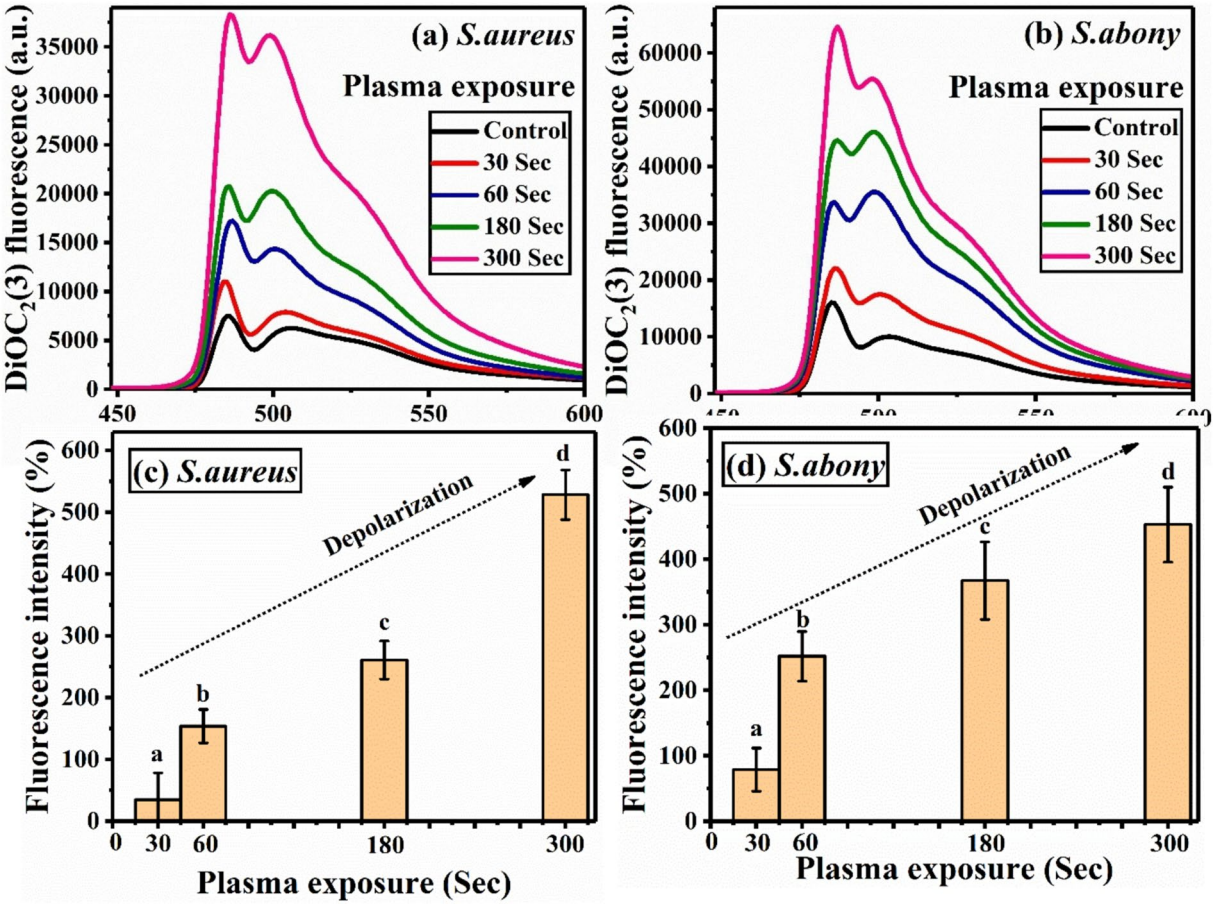

Fig. 12. Fluorescence spectra of $DiOC_2(3)$ stained (**a**) *S. aureus*, & (**b**) *S. abony* bacterial samples following plasma treatment for measuring the membrane potential, quantification of fluorescence intensity (%) for (**c**) *S. aureus*, & (**d**) *S. abony* indicating membrane depolarization.

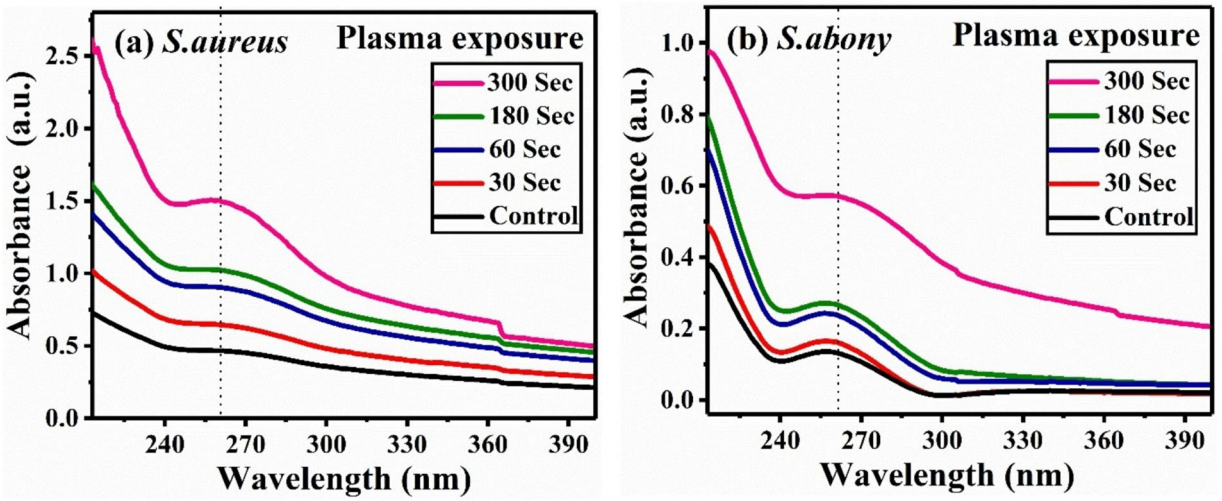

Fig. 13. UV absorbance spectra of plasma treated (**a**) *S. aureus* and (**b**) *S. abony* showing intracellular DNA damage and hyperchromic effect.

of plasma treatment, indicating a gradual leakage of DNA from both *S. aureus* and *S. abony*. In contrast, the concentration of proteins leaked into the suspension after plasma treatment may be below the detection threshold of the spectrophotometer at 280 nm. Unlike DNA, proteins have comparatively weaker absorbance unless present in large concentrations. However, their leakage is confirmed through ATR-FTIR analysis based on molecular vibration signatures in the subsequent section[73]. The increase in ultraviolet light absorbance in double-stranded DNA underscores the hyperchromic effect or shift, signifying structural alterations and denaturation of DNA molecules following plasma treatment[74]. DNA comprises two complementary strands that are bound together by hydrogen bonds formed between paired nucleotide bases. Denaturation of DNA occurs when these hydrogen bonds break, leading to the separation of the two strands. This structural shift often results increase in absorption of UV light. Chauvin et al. reported that H_2O_2 serves as a central genotoxic agent produced during plasma exposure. This genotoxicity is attributed to H_2O_2's ability to diffuse through cell membranes and generate $^{\cdot}OH$ via a Fenton reaction catalysed by iron-containing proteins[75]. The high reactivity of $^{\cdot}OH$ with cellular components confers a potent capacity to induce DNA damage, including the oxidation of nucleobase pairs (A–T and G–C) and DNA cleavage, leading to cell death. Additionally, these damaged bases become unstacked and exhibit increased light absorption. An insightful review by Arjunan et al. also suggests that reactive species generated during atmospheric pressure plasma exposure contribute to DNA denaturation and oxidation, thereby enhancing the efficacy of plasma treatment for sterilization purposes[76]. Similarly, microwave plasma impacts the DNA of both *S. aureus* and *S. abony*, mediated by the presence of H_2O_2 and $^{\cdot}OH$ radicals. However, differences in DNA repair mechanisms between *S. aureus* and *S. abony* may result in varying efficiency and capacity for repairing plasma-induced oxidative damage, which is reflected in the distinct absorbance values observed for both bacterial samples.

Molecular changes and leakage analysis using ATR-FTIR

Bacterial cells encapsulate a diverse group of bio-molecules, comprising proteins, lipids, nucleic acids, and carbohydrates, each exhibiting characteristic absorption bands in the infrared spectrum. Investigation via ATR-FT-IR spectroscopy of plasma-treated bacterial specimens offers valuable insights into the alterations and leakage phenomena affecting associated functional groups presents in bacteria following plasma exposure[43]. Figure 14a delineates the FT-IR spectra of *S. aureus* acquired within the wavenumber range of 900–4000 cm^{-1} across varied plasma treatment durations. Additionally, Fig. 14b,c exhibit high-resolution ATR-FTIR spectra of *S. aureus* recorded within the wavenumber ranges of 1000–1800 cm^{-1} and 2600–4000 cm^{-1}, respectively. Upon spectral analysis, discernible shifts and enhancements in peaks associated with crucial molecular entities signify leakage from the intracellular location of bacteria, thereby resulting in heightened peak intensities. Notably, bacterial suspensions prepared in PBS evince a greater leaked biomolecules subsequent to plasma treatment compared to untreated sample. The emergence of altered bands, such as those at 1016 and 1054 cm^{-1}, linked to $\nu_s(PO_2)$ nucleic acid and phospholipids, respectively, indicates the release of nucleic acid constituents from both *S. aureus* and *S. abony* depicted in Figs. 14b and 15b, respectively[77].

Moreover, the relocation of the 1642 cm^{-1} band attributed to amide I (predominantly C=O stretching of proteins) underscores structural modifications[43,78]. The shift towards higher wavenumbers of the 2870 cm^{-1} peak, assigned to $\nu_{as}(CH_2)$ (mainly proteins), reflects protein denaturation consequent to molecular mass reduction[79]. Asymmetric bands at 2924 and 2973 cm^{-1}, pertaining mainly to lipids and fatty acids, exhibit conspicuous alterations owing to interactions with reactive species[80]. Similarly, the 3317 cm^{-1} band, primarily ascribed to ν(NH) within the amide A region of proteins, shows a shift towards lower wavenumbers . Also, the characteristic peaks indicative of O–H stretching is appeared at 3648 cm^{-1} within water containing-PBS solutions[81].

Similarly, Fig. 15a represents the IR spectra of *S. abony* measured in the wavenumber range of 900–4000 cm^{-1}, exposed to different plasma treatment times. Similar alterations in peak intensities and shifts are observed in plasma-treated *S. abony* samples akin to those noted in *S. aureus*. Figure 15b depicts high-resolution spectra of *S. abony* recorded in the wavenumber range of 1000–1800 cm^{-1}, with bands at 1016, 1054, and 1650 cm^{-1} showing alteration affiliated with $\nu_s(PO_2)$ nucleic acid, phospholipids, and the amide I region, respectively[78]. This spectra also suggesting cellular DNA leakage, the peak at 1650 cm^{-1} signifies vibrations of C_6=O in guanine and C_4=O in thymine DNA bases[82]. Figure 15c illustrates high-resolution spectra of *S. abony* recorded in the wavenumber range of 2600–4000 cm^{-1}, with absorption peaks at 2860, 2921, and 2976 cm^{-1} assigned to $\nu_s(CH_2)$, $\nu_{as}(CH_2)$, and $\nu_{as}(CH_3)$, respectively[43,83]. Noticeable peak shifts and enhancements are observed in the above-mentioned molecular conformations, indicating leakage of lipids and proteins. The major peak shift was observed for N–H stretching of proteins at 3235 cm^{-1} along with the O–H stretching band at 3692 cm^{-1} in *S. abony*[29,43].

In summation, the excessive generation of reactive species, notably $^{\cdot}OH$ and H_2O_2, elicits detrimental effects on all biomolecular constituents including proteins, lipids, DNA, and carbohydrates within both *S. aureus* and *S. abony*. Protein oxidation catalysed by reactive species leads to peptide chain cleavage and protein conversion into derivatives susceptible to proteolytic degradation[84]. The discernible intensity augmentation across all peaks, as characterized by FT-IR spectra of both bacterial samples, underscores cell lysis and the release or leakage of intracellular contents into the bacterial suspension, as corroborated by strong absorption bands in the FTIR spectra. The peak height or band area reflected the concentration of the functional groups whereas frequency values associated with IR bands elucidated the molecular conformation. Surprisingly, no existing bands disappeared, nor did new bands appear in the spectral analysis. Importantly, the severity of leakage escalates with prolonged treatment durations.

Conclusion

This paper aimed to develop a non-thermal microwave plasma sterilization system using a microwave source with an air and ozone mixture and to evaluate the effectiveness of microwave plasma in inactivating bacteria. The high plasma density from the microwave source was found to significantly contribute to the 6-log reduction

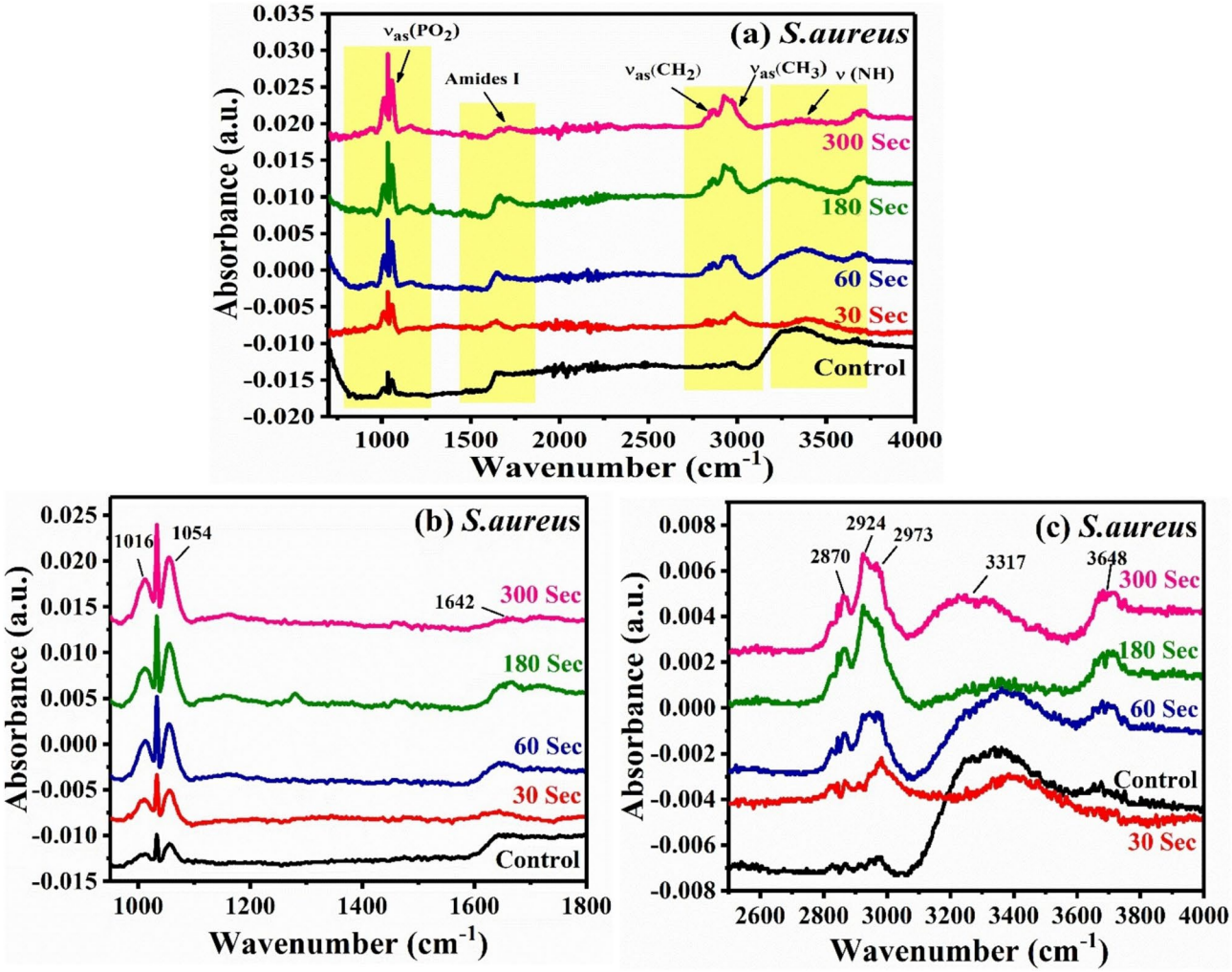

Fig. 14. ATR FTIR spectra of plasma treated (**a**) *S. aureus*. The spectral range is 1000–4000 cm^{-1}, (**b**) 1000–1800 (**c**) 2600–4000 cm^{-1}.

of *S. aureus* and *S. abony*, as demonstrated by the conventional colony count method. The study suggests that bacterial inactivation likely occurs due to the diffusion of highly and intense amount of reactive oxygen species, such as $^{\cdot}OH$ and H_2O_2, which create oxidative stress within the bacterial cells. To gain a deeper understanding of the bacterial cell death and inactivation mechanisms, various spectroscopic and microscopic methods were employed. Notable findings included (i) leakage of inner cellular contents, (ii) hyperchromic shift of double stranded DNA, (iii) membrane depolarization and change in membrane potential, (iv) a decrease in viable cell counts, (v) noticeable morphological changes were observed such as, pore formation, cellular expansion, high surface roughness, and irregular shapes etc. and (vi) an increase in the number of propidium iodide stained dead red fluorescent cells. Overall, our study demonstrated the excellent antibacterial activity of non-thermal microwave plasma against *S. aureus* and *S. abony*. Future research on the potential of plasma sterilization needs to focus on its effectiveness, scalability, and application in the healthcare sector. Studies could further explore the optimization of plasma parameters for cost-effective rapid sterilization of medical and surgical instruments, biofilm removal, and surface decontamination in hospitals ensuring a safer, healthier future for all.

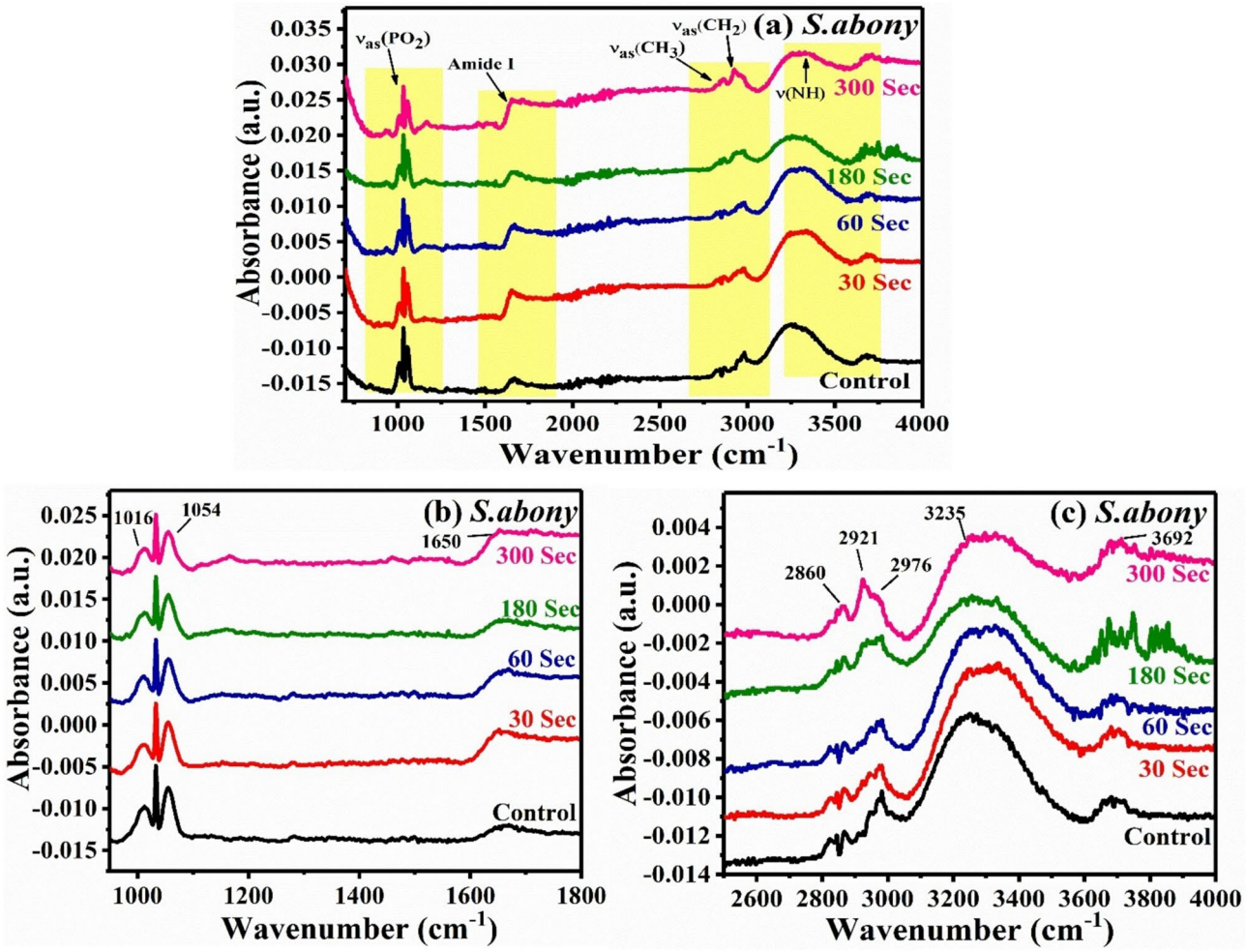

Fig. 15. ATR FTIR spectra of plasma treated (**a**) *S. abony*. The spectral range is 1000–4000 cm^{-1}, (**b**) 1000–1800 (**c**) 2600–4000 cm^{-1}.

Data availability

The corresponding author can provide the data supporting this study's findings upon reasonable request.

Received: 1 January 2025; Accepted: 13 May 2025
Published online: 24 May 2025

References

1. Sakudo, A., Yagyu, Y. & Onodera, T. Disinfection and sterilization using plasma technology: Fundamentals and future perspectives for biological applications. *Int. J. Mol. Sci.* **20**(20), 5216 (2019).
2. Moisan, M. et al. Plasma sterilization. Methods and mechanisms. *Pure Appl. Chem.* **74**(3), 349–358 (2002).
3. Akter, M., Yadav, D. K., Ki, S. H., Choi, E. H. & Han, I. Inactivation of infectious bacteria using nonthermal biocompatible plasma cabinet sterilizer. *Int. J. Mol. Sci.* **21**(21), 8321 (2020).
4. Klämpfl, T. G. et al. Cold atmospheric air plasma sterilization against spores and other microorganisms of clinical interest. *Appl. Environ. Microbiol.* **78**(15), 5077–5082 (2012).
5. Schaal, T. & Schmelz, U. Plasma disinfection procedures for surfaces in emergency service vehicles: A field trial at the German Red Cross. *Sci. Rep.* **13**(1), 20737 (2023).
6. Lerouge, S., Wertheimer, M. R. & Yahia, L. H. Plasma sterilization: A review of parameters, mechanisms, and limitations. *Plasmas Polym.* **6**, 175–188 (2001).
7. Sakudo, A., Yamashiro, R. & Onodera, T. Recent advances in prion inactivation by plasma sterilizer. *Int. J. Mol. Sci.* **23**(18), 10241 (2022).
8. Soni, A., Smith, J., Thompson, A. & Brightwell, G. Microwave-induced thermal sterilization-A review on history, technical progress, advantages and challenges as compared to the conventional methods. *Trends Food Sci. Technol.* **97**, 433–442 (2020).
9. Kaushik, N. et al. The inactivation and destruction of viruses by reactive oxygen species generated through physical and cold atmospheric plasma techniques: Current status and perspectives. *J. Adv. Res.* **43**, 59–71 (2023).
10. Nicol, M. J. et al. Antibacterial effects of low-temperature plasma generated by atmospheric-pressure plasma jet are mediated by reactive oxygen species. *Sci. Rep.* **10**(1), 3066 (2020).
11. Stoffels, E., Sakiyama, Y. & Graves, D. B. Cold atmospheric plasma: Charged species and their interactions with cells and tissues. *IEEE Trans. Plasma Sci.* **36**(4), 1441–1457 (2008).

12. Zhang, H. et al. Roles of membrane protein damage and intracellular protein damage in death of bacteria induced by atmospheric-pressure air discharge plasmas. *RSC Adv.* **8**(38), 21139–21149 (2018).
13. Arjunan, K. P., Sharma, V. K. & Ptasinska, S. Effects of atmospheric pressure plasmas on isolated and cellular DNA-a review. *Int. J. Mol. Sci.* **16**(2), 2971–3016 (2015).
14. Qian, J., Wang, C., Zhuang, H., Zhang, J. & Yan, W. Oxidative stress responses of pathogen bacteria in poultry to plasma-activated lactic acid solutions. *Food Control* **118**, 107355 (2020).
15. Mai-Prochnow, A., Murphy, A. B., McLean, K. M., Kong, M. G. & Ostrikov, K. K. Atmospheric pressure plasmas: Infection control and bacterial responses. *Int. J. Antimicrob. Agents* **43**(6), 508–517 (2014).
16. Gaunt, L. F., Beggs, C. B. & Georghiou, G. E. Bactericidal action of the reactive species produced by gas-discharge nonthermal plasma at atmospheric pressure: A review. *IEEE Trans. Plasma Sci.* **34**(4), 1257–1269 (2006).
17. Weltmann, K. D. & Von Woedtke, T. Basic requirements for plasma sources in medicine. *The European Physical Journal-Applied Physics* **55**(1), 13807 (2011).
18. Menashi, W. P. Treatment of surfaces. US Patent 3,383,163 (1968).
19. Ganguli, A. & Tarey, R. D. Understanding plasma sources, current science special section: Plasma applications. **83**(3), 279–290 (2002).
20. Moisan, M. et al. Low-temperature sterilization using gas plasmas: A review of the experiments and an analysis of the inactivation mechanisms. *Int. J. Pharm.* **226**(1–2), 1–21 (2001).
21. Todorova, Y. et al. Non-thermal atmospheric plasma for microbial decontamination and removal of hazardous chemicals: An overview in the circular economy context with data for test applications of microwave plasma torch. *Processes* **10**(3), 554 (2022).
22. Latrasse, L., Lacoste, A., Sirou, J. & Pelletier, J. High density distributed microwave plasma sources in a matrix configuration: Concept, design and performance. *Plasma Sources Sci. Technol.* **16**(1), 7 (2006).
23. Popov, O. A. *High Density Plasma Sources: Design, Physics and Performance* (Elsevier, 1996).
24. Renoux, L. et al. Use of a microwave plasma process at atmospheric pressure for bacterial inactivation without thermal effects. *Mater. Sci. Appl.* **14**(5), 285–298 (2023).
25. Handorf, O. et al. Antimicrobial effects of microwave-induced plasma torch (MiniMIP) treatment on *Candida albicans* biofilms. *Microb. Biotechnol.* **12**(5), 1034–1048 (2019).
26. Moreau, S. et al. Using the flowing afterglow of a plasma to inactivate *Bacillus subtilis* spores: Influence of the operating conditions. *J. Appl. Phys.* **88**(2), 1166–1174 (2000).
27. Seo, S. H. et al. Antibacterial activity and effect on gingival cells of microwave-pulsed non-thermal atmospheric pressure plasma in artificial saliva. *Sci. Rep.* **7**(1), 8395 (2017).
28. Kim, E. J., Hyun, J. E., Kang, Y. H., Baek, S. J. & Hwang, C. Y. *In vitro* antibacterial and antibiofilm effects of cold atmospheric microwave plasma against Pseudomonas aeruginosa causing canine skin and ear infections. *Vet. Dermatol.* **33**(1), 29 (2022).
29. Barkhade, T., Nigam, K., Ravi, G., Rawat, S. & Nema, S. K. Plasma sterilization for bacterial inactivation: Studies on probable mechanisms and biochemical actions. *Plasma Chem. Plasma Process.* **44**(1), 429–454 (2024).
30. Zhao, J. & Nie, L. Five gaseous reactive oxygen and nitrogen species (RONS) density generated by microwave plasma jet. *Phys. Plasmas* https://doi.org/10.1063/1.5092840 (2019).
31. Mastanaiah, N., Banerjee, P., Johnson, J. A. & Roy, S. Examining the role of ozone in surface plasma sterilization using dielectric barrier discharge (DBD) plasma. *Plasma Processes Polym.* **10**(12), 1120–1133 (2013).
32. Thai, V. P., Dam, T. N., Takahashi, K., Sasaki, T., & Kikuchi, T. The generation pathways of OH and H_2O_2 by plasma-liquid interactions. In *IOP Conference Series Earth and Environmental Science* Vol. 1278, No. 1, p. 012030 (IOP Publishing, 2023).
33. Ueda, D. et al. Sterilization of underwater bacteria by ozone bubble pulsed discharge. *IEEE Trans. Plasma Sci.* **51**(2), 333–341 (2022).
34. Deeba, F., Qayyum, A. & Mahmood, N. Optical emission spectroscopy of 245 GHz microwave induced plasma. *J. Res. Spectrosc.* **2015**, 172302 (2015).
35. Figge, M. J., Robertson, L. A., Ast, J. C. & Dunlap, P. V. Historical microbiology: Revival and phylogenetic analysis of the luminous bacterial cultures of MW Beijerinck. *FEMS Microbiol. Ecol.* **78**(3), 463–472 (2011).
36. Sobhan, A., Sher, M., Muthukumarappan, K., Zhou, R. & Wei, L. Cold plasma treatment for *E. coli* inactivation and characterization for fresh food safety. *J. Agric. Food Res.* **18**, 101403 (2024).
37. Liao, C. H. & Shollenberger, L. M. Survivability and long-term preservation of bacteria in water and in phosphate-buffered saline. *Lett. Appl. Microbiol.* **37**(1), 45–50 (2003).
38. Lv, X. & Cheng, J. H. Evaluation of the effects of cold plasma on cell membrane lipids and oxidative injury of *Salmonella typhimurium*. *Molecules* **27**(3), 640 (2022).
39. Khater, M., Khater, S. S., Gholap, H., Patil, R. & Kulkarni, G. Comparative studies on measurement of membrane potential of bacterial cells treated with ZnO nanoparticles by spectrofluorometry, fluorescence microscopy and flowcytometry. *J. Microbiol. Methods* **173**, 105920 (2020).
40. Paparella, A. et al. Flow cytometric assessment of the antimicrobial activity of essential oils against Listeria monocytogenes. *Food Control* **19**(12), 1174–1182 (2008).
41. Nguyen, N. H. B., Pham, T. T. V., Huynh, T. Q., Nguyen, T. H. & Nguyen, T. T. H. Sample preparative procedure for Pseudomonas aeruginosa observation under scanning electron microscope. *Vietnam J. Biotechnol.* **20**(4), 717–726 (2022).
42. McFeters, G. A., Feipeng, P. Y., Pyle, B. H. & Stewart, P. S. Physiological assessment of bacteria using fluorochromes. *J. Microbiol. Methods* **21**(1), 1–13 (1995).
43. Zhang, L., Wang, H. & Luo, H. Uncovering the inactivation kinetics of *Escherichia coli* in saline by atmospheric DBD plasma using ATR FT-IR. *Plasma Processes Polym.* **17**(9), 1900197 (2020).
44. Shintani, H., Sakudo, A., Burke, P. & McDonnell, G. Gas plasma sterilization of microorganisms and mechanisms of action. *Exp. Ther. Med.* **1**(5), 731–738 (2010).
45. Kramida, A., Ralchenko, Y., Reader, J. & NIST ASD Team. *NIST Atomic Spectra Database (version 5.10)*. (National Institute of Standards and Technology, Gaithersburg).
46. Boehm, D., Heslin, C., Cullen, P. J. & Bourke, P. Cytotoxic and mutagenic potential of solutions exposed to cold atmospheric plasma. *Sci. Rep.* **6**(1), 21464 (2016).
47. Mai-Prochnow, A., Clauson, M., Hong, J. & Murphy, A. B. Gram positive and Gram negative bacteria differ in their sensitivity to cold plasma. *Sci. Rep.* **6**(1), 38610 (2016).
48. Flynn, P. B. et al. Bactericidal efficacy of atmospheric pressure non-thermal plasma (APNTP) against the ESKAPE pathogens. *Int. J. Antimicrob. Agents* **46**(1), 101–107. https://doi.org/10.1016/j.ijantimicag.2015.02.026 (2015).
49. Montie, T. C., Kelly-Wintenberg, K. & Roth, J. R. An overview of research using the one atmosphere uniform glow discharge plasma (OAUGDP) for sterilization of surfaces and materials. *IEEE Trans. Plasma Sci.* **28**(1), 41–50 (2000).
50. Park, B. J. et al. Escherichia coli sterilization and lipopolysaccharide inactivation using microwave-induced argon plasma at atmospheric pressure. *Surf. Coat. Technol.* **201**(9–11), 5738–5741 (2007).
51. Bienert, G. P. et al. Specific aquaporins facilitate the diffusion of hydrogen peroxide across membranes. *J. Biol. Chem.* **282**(2), 1183–1192 (2007).
52. Lim, J., Park, S., Ryu, S., Park, S. & Kim, M. S. Different inactivation mechanisms of *Staphylococcus aureus* and *Escherichia coli* in water by reactive oxygen and nitrogen species generated from an argon plasma jet. *Environ. Sci. Technol.* **59**, 3276–3285 (2025).

53. Brignoli, T. et al. Wall teichoic acids facilitate the release of toxins from the surface of Staphylococcus aureus. *Microbiol. Spectr.* **10**(4), e01011–e01022 (2022).
54. Graves, D. B. The emerging role of reactive oxygen and nitrogen species in redox biology and some implications for plasma applications to medicine and biology. *J. Phys. D Appl. Phys.* **45**(26), 263001 (2012).
55. Mouele, E. S. M. et al. A critical review on ozone and co-species, generation and reaction mechanisms in plasma induced by dielectric barrier discharge technologies for wastewater remediation. *J. Environ. Chem. Eng.* **9**(5), 105758 (2021).
56. Kremer, M. L. Initial steps in the reaction of H_2O_2 with Fe^{2+} and Fe^{3+} ions: Inconsistency in the free radical theory. *Reactions* **4**(1), 171–175 (2023).
57. Lee, G. J., Sim, G. B., Choi, E. H., Kwon, Y. W., Kim, J. Y., Jang, S., & Kim, S. H. Optical and structural properties of plasma-treated Cordyceps bassiana spores as studied by circular dichroism, absorption, and fluorescence spectroscopy. *J. Appl. Phys.* **117**(2). (2015).
58. Vergalli, J. et al. Porins and small-molecule translocation across the outer membrane of Gram-negative bacteria. *Nat. Rev. Microbiol.* **18**(3), 164–176 (2020).
59. Samanta, A., Paul, B. K. & Guchhait, N. Photophysics of DNA staining dye Propidium iodide encapsulated in bio-mimetic micelle and genomic fish sperm DNA. *J. Photochem. Photobiol. B* **109**, 58–67 (2012).
60. Deng, Y., Wang, L., Chen, Y. & Long, Y. Optimization of staining with SYTO 9/propidium iodide: Interplay, kinetics and impact on Brevibacillus brevis. *Biotechniques* **69**(2), 88–98 (2020).
61. Zhang, G. E., Meredith, T. C. & Kahne, D. On the essentiality of lipopolysaccharide to gram-negative bacteria. *Curr. Opin. Microbiol.* **16**(6), 779–785 (2013).
62. Chan, L. W. et al. Selective permeabilization of gram-negative bacterial membranes using multivalent peptide constructs for antibiotic sensitization. *ACS Infect. Dis.* **7**(4), 721–732 (2021).
63. Dolezalova, E. & Lukes, P. Membrane damage and active but non-culturable state in liquid cultures of *Escherichia coli* treated with an atmospheric pressure plasma jet. *Bioelectrochemistry* **103**, 7–14 (2015).
64. Cossarizza, A. et al. Guidelines for the use of flow cytometry and cell sorting in immunological studies. *Eur. J. Immunol.* **49**(10), 1457–1973 (2019).
65. Sharkey, M. A., Chebbi, A., McDonnell, K. A., Staunton, C. & Dowling, D. P. Evaluation of the sensitivity of bacterial and yeast cells to cold atmospheric plasma jet treatments. *Biointerphases* **10**(2), 029507 (2015).
66. Sachidanandham, R., Yew-Hoong Gin, K. & Laa Poh, C. Monitoring of active but non-culturable bacterial cells by flow cytometry. *Biotechnol. Bioeng.* **89**(1), 24–31 (2005).
67. Liao, X., Liu, D. & Ding, T. Non-thermal plasma induces the viable-but-nonculturable state in *Staphylococcus aureus* via metabolic suppression and the oxidative stress response. *Appl. Environ. Microbiol.* **86**(5), e02216–e02219 (2020).
68. Takamatsu, T. et al. Imaging of the Staphylococcus aureus inactivation process induced by a multigas plasma jet. *Curr. Microbiol.* **73**, 766–772 (2016).
69. Shi, X. et al. Development and characterization of touchable air plasma jet device for inactivation of oral bacteria. *Results Phys.* **36**, 105405 (2022).
70. Dezest, M. et al. Oxidative modification and electrochemical inactivation of *Escherichia coli* upon cold atmospheric pressure plasma exposure. *PLoS ONE* **12**(3), e0173618 (2017).
71. Te Winkel, J. D., Gray, D. A., Seistrup, K. H., Hamoen, L. W. & Strahl, H. Analysis of antimicrobial-triggered membrane depolarization using voltage sensitive dyes. *Front. Cell Dev. Biol.* **4**, 29 (2016).
72. Lo, W. C., Krasnopeeva, E. & Pilizota, T. Bacterial electrophysiology. *Annu. Rev. Biophys.* **53**, 487–510 (2024).
73. Kong, J. & Yu, S. Fourier transform infrared spectroscopic analysis of protein secondary structures. *Acta Biochim. Biophys. Sin.* **39**(8), 549–559 (2007).
74. D'Abramo, M., Castellazzi, C. L., Orozco, M. & Amadei, A. On the nature of DNA hyperchromic effect. *J. Phys. Chem. B* **117**(29), 8697–8704 (2013).
75. Chauvin, J., Judée, F., Yousfi, M., Vicendo, P. & Merbahi, N. Analysis of reactive oxygen and nitrogen species generated in three liquid media by low temperature helium plasma jet. *Sci. Rep.* **7**(1), 1–15 (2017).
76. Arjunan, K. P., Sharma, V. K. & Ptasinska, S. Effects of atmospheric pressure plasmas on isolated and cellular DNA—a review. *Int. J. Mol. Sci.* **16**(2), 2971–3016 (2015).
77. Jiang, W., Yang, K., Vachet, R. W. & Xing, B. Interaction between oxide nanoparticles and biomolecules of the bacterial cell envelope as examined by infrared spectroscopy. *Langmuir* **26**, 18071–18077 (2010).
78. Quilès, F., Humbert, F. & Delille, A. Analysis of changes in attenuated total reflection FTIR fingerprints of Pseudomonas fluorescens from planktonic state to nascent biofilm state. *Spectrochim. Acta Part A Mol. Biomol. Spectrosc.* **75**(2), 610–616 (2010).
79. Nadtochenko, V. A., Rincon, A. G., Stanca, S. E. & Kiwi, J. Dynamics of *E. coli* membrane cell peroxidation during TiO_2 photocatalysis studied by ATR-FTIR spectroscopy and AFM microscopy. *J. Photochem. Photobiol. A Chem.* **169**(2), 131–137 (2005).
80. Kiwi, J. & Nadtochenko, V. Evidence for the mechanism of photocatalytic degradation of the bacterial wall membrane at the TiO_2 interface by ATR-FTIR and laser kinetic spectroscopy. *Langmuir* **21**(10), 4631–4641 (2005).
81. Naumann, D., Helm, D. & Labischinski, H. Microbiological characterizations by FT-IR spectroscopy. *Nature* **351**(6321), 81–82 (1991).
82. Piccirilli, F. et al. Infrared Nanospectroscopy reveals DNA structural modifications upon immobilization onto clay nanotubes. *Nanomaterials* **11**(5), 1103. https://doi.org/10.3390/nano11051103 (2021).
83. Naumann, D. Infrared spectroscopy in microbiology. *Encycl. Anal. Chem.* **102**, 131 (2000).
84. Cecarini, V. et al. Protein oxidation and cellular homeostasis: Emphasis on metabolism. *Biochim. Biophys. Acta (BBA) Mol. Cell Res.* **1773**(2), 93–104 (2007).

Acknowledgements

The authors are very grateful to School of Life Sciences, Central University of Gujarat, Gandhinagar, India for providing the necessary laboratory and instrumentation facilities for carrying out post plasma treatment experiments. Authors also thankful to central Instrumentation facility at Indian Institute of Technology, Gandhinagar for availing imaging facilities.

Author contributions

T.B., K.N., G.R., and S.K.N. contributed to the study's conceptualization. T.B. managed material preparation, data collection, and analysis. T.B. drafted the main manuscript text, with G.R., K.N., S.R., and S.K.N. offering feedback on revised versions. K.N. and G.R. were responsible for designing and developing the plasma system. All authors reviewed and approved the final manuscript.

Funding
Open access funding provided by Department of Atomic Energy.

Declarations

Competing interests
The authors declare no competing interests.

Additional information
Correspondence and requests for materials should be addressed to T.B.

Reprints and permissions information is available at www.nature.com/reprints.

Publisher's note Springer Nature remains neutral with regard to jurisdictional claims in published maps and institutional affiliations.